

# Hubble Space Telescope Imaging of Globular Cluster Candidates in Low Surface Brightness Dwarf Galaxies<sup>\*</sup>

M. E. Sharina<sup>1,2</sup>, T. H. Puzia<sup>3,\*\*</sup>, and D. I. Makarov<sup>1,2</sup>

<sup>1</sup> Special Astrophysical Observatory, Russian Academy of Sciences, N. Arkhyz, KChR, 369167, Russia

<sup>2</sup> Isaac Newton Institute, Chile, SAO Branch

<sup>3</sup> Space Telescope Science Institute, 3700 San Martin Drive, Baltimore, MD21218, USA

Received: February 2005 – Accepted: May 2005

**Abstract.** Fifty-seven nearby low surface brightness dwarf galaxies ( $-10 \gtrsim M_V \gtrsim -16$ ) were searched for globular cluster candidates (GCCs) using *Hubble Space Telescope* WFPC2 imaging in  $V$  and  $I$ . The sample consists of 18 dwarf spheroidal (dSph), 36 irregular (dIrr), and 3 "transition" type (dIrr/dSph) galaxies with angular sizes less than 3.7 kpc situated at distances 2–6 Mpc in the field and in the nearby groups: M81, Centaurus A, Sculptor, Canes Venatici I cloud. We find that  $\sim 50\%$  of dSph, dIrr/dSph, and dIrr galaxies contain GCCs. The fraction of GCCs located near the center of dwarf spheroidal galaxies is  $\gtrsim 2$  times higher than that for dIrrs. The mean integral color of GCCs in dSphs,  $(V - I)_0 = 1.04 \pm 0.16$  mag, coincides with the corresponding value for Galactic globular clusters and is similar to the *blue* globular cluster sub-populations in massive early-type galaxies. The color distribution for GCCs in dIrrs shows a clear bimodality with peaks near  $(V - I)_0 = 0.5$  and 1.0 mag. Blue GCCs are presumably young with ages  $t \lesssim 1$  Gyr, while the red GCC population is likely to be older. The detected GCCs have absolute visual magnitudes between  $M_V = -10$  and  $-5$  mag. We find indications for an excess population of faint GCCs with  $M_V \gtrsim -6.5$  mag in both dSph and dIrr galaxies, reminiscent of excess populations of faint globular clusters in nearby Local Group spiral galaxies. The measurement of structural parameters using King-profile fitting reveals that most GCCs have structural parameters similar to extended outer halo globular clusters in the Milky Way and M31, as well as the recently discovered population of "faint fuzzy" clusters in nearby lenticular galaxies.

**Key words.** galaxies: photometry — dwarf — galaxies — star clusters

## 1. Introduction

Low surface brightness dwarf galaxies ( $M_V > -16$ , and central surface brightness  $\mu_V \gtrsim 22$  mag/arcsec<sup>2</sup>) constitute the most numerous galaxy type in the local universe. Their formation mechanisms, their physical structure, and their contribution to the assembly of massive galaxies has attracted great attention since many years (e.g. Ferguson & Binggeli 1994; Impey & Bothun 1997; Bothun et al. 1997; Klypin et al. 1999; Kravtsov et al. 2004). Star formation in these low-mass stellar systems appears to be governed by a complex interplay of gravitational instabilities, turbulence, and gas thermodynamics (e.g. Elmegreen 2002; Pelupessy et al. 2004). In extreme cases, star formation culminates in the formation of massive star clusters that are likely to be the

young counterparts of today's old globular clusters (e.g. Larsen & Richtler 2000). This mode of star-formation is observed in numerous nearby dwarf irregular galaxies (dIrr; e.g. Billett et al. 2002; Hunter & Elmegreen 2004), but appears to have ceased a long time ago in dwarf spheroidal (dSph) and dwarf elliptical galaxies (dE; see Lotz et al. 2004)<sup>1</sup>. While dE and dSph galaxies are predominantly found in the vicinity of massive galaxies in galaxy groups and rich galaxy clusters, dIrr galaxies are predominantly located in the field and in loose groups. The conditions for globular cluster formation in dwarf galaxies at a given galaxy mass might be therefore a sensitive function of environmental density. It is still not clear whether dE, dSph, and dIrr share similar formation and/or early evolution histories (Davies & Phillipps 1988; Marlowe et al. 1999). However, the three galaxy types share one property: they all harbor globular clusters that are older than several Gyr, which indicates that at least

<sup>\*</sup> Based on observations made with the NASA/ESA Hubble Space Telescope. The Space Telescope Science Institute is operated by the Association of Universities for Research in Astronomy, Inc. under NASA contract NAS 5-26555.

<sup>\*\*</sup> ESA Fellow, Space Telescope Division of ESA

<sup>1</sup> We explicitly consider in our sample the type of tidal dwarf galaxies (e.g. Weibacher 2002).

early globular cluster formation took place irrespective of the morphological type. One can use these globular clusters to investigate the early star formation and chemical evolution histories of these galaxies. Because they are composed of stars of one age and chemical composition, globular clusters offer a unique tool to access the star formation histories of individual galaxies (e.g. Ashman & Zepf 1998; Kissler-Patig 2000; Harris 2001).

In the present epoch, the formation of massive bound star clusters seems to be associated with high-pressure environment and powerful star formation events (e.g. Elmegreen & Efremov 1997; Ashman & Zepf 2001). High-pressure environment naturally occurs in dwarf galaxies due to their low metallicities and high critical densities for star formation. Since globular clusters sample the chemical conditions during major star formation events in a galaxy, the chemical composition of globular clusters in dE, dSph, and dIrr galaxies might provide crucial information on star formation histories and mechanisms that are important inputs for hierarchical galaxy formation models. We therefore embarked on a spectroscopic survey of globular clusters in nearby low surface brightness galaxies in and outside the Local Group (LG).

In this paper, we present the photometric study of globular cluster candidates. In Section 2 we describe the galaxy sample and data reduction steps. Section 3 deals with the cluster candidate selection, while in Section 4 we investigate the properties of the globular cluster candidates (GCCs).

## 2. Observations and Data Reduction

Before discussing the properties of globular cluster candidates in nearby dwarf galaxies, we briefly summarize the main characteristics of the objects of interest. Globular clusters are centrally concentrated, mostly spherical systems with masses of  $10^4 \leq M_{\odot} \leq 10^{6.6}$ , luminosities from  $M_V = -10.55$  (Mayall II in M31) to  $+0.2$  mag (AM-4 in the Milky Way), and half-light radii ranging from  $\sim 0.3$  to  $\sim 25$  pc. They are bound objects whose lifetimes may exceed a Hubble time. So far, globular clusters have been detected in 12 of the 36 Local Group galaxies (Hodge et al. 2002). Table 1 presents a list of galaxies that were searched for globular cluster candidates in this study.

Numerical values in the columns 3–4 and 6–8 were extracted and/or computed from data presented in Karachentsev et al. (2004). Surveying Table 1 shows that our sample is composed of 18 dwarf spheroidal (dSph:  $T < -1$ ), 36 dwarf irregular (dIrr:  $T > 9$ ), and 3 intermediate-type (dSph/dIrr:  $T = -1$ ) galaxies with mean surface brightnesses  $\mu_B > 23$  mag/arcsec<sup>2</sup> and angular sizes less than 3.7 kpc. All galaxies, except KK84<sup>2</sup>, are situated at distances  $\sim 2$ –6 Mpc in the field and in the nearby groups: M81, Centaurus A, Sculptor, Canes Venatici I cloud (see Tab. 2 for details). We find globular cluster candidates in 10 of 18 dSphs, 18 of 36 dIrrs, and 2 of 3 intermediate-type

dwarfs. In general, roughly 50% of all surveyed galaxies contain globular cluster candidates, irrespective of morphological type.

The galaxies were surveyed with the HST Wide Field and Planetary Camera 2 (WFPC2; snapshot programs GO-8192, GO-8601) with 600-second exposures taken in the F606W and F814W filters for each object. Accurate distances to 111 nearby galaxies were determined in these snapshot programs (e.g. Karachentsev et al. 2003) and provide us an unique benchmark to study properties of globular cluster systems in a number of low surface brightness dwarf galaxies. Karachentsev et al. (2001a) searched for globular cluster candidates in dSph galaxies of the M81 group. We extend this work using our selection criteria and include also other low-mass galaxies in this sample. In general, surveying virtually the full area of all our dwarf galaxies, given their relatively small angular sizes of  $\lesssim 2'$ , allows us to study the spatial distribution of globular cluster candidates.

In the following we briefly discuss a few particularly interesting galaxies. WFPC2 images with marked GCCs in UGC 3755 and Holmberg IX are shown in Figure 1a,b. These two galaxies, which have different properties and are located in different environments (see Tab. 2), have the largest numbers of globular cluster candidates among our sample galaxies. UGC 3755 is an isolated dwarf irregular galaxy (Karachentsev et al. 2004). Holmberg IX is a tidal dwarf companion of M81 (Yun et al. 1994; Boyce et al. 2001). We searched for globular cluster candidates in other tidal dwarf companions of M81, namely BK3N, Arp-loop (A0952+69) and Garland, but found no GCCs in these galaxies. A faint GCC ( $M_{V,0} = -5.2$ ) in BK3N is located outside the boundary of the galaxy and probably belongs to M81. Six dSph galaxies contain GCCs located near their centers. KK84 and KK221 have the largest number of GCCs among our dSph sample (see Tab. 2 and Figure 1 c,d). Overplotted on Figure 1d is the isophote of constant surface brightness  $\mu_B \sim 26.5$  mag/arcsec<sup>2</sup>. All globular cluster candidates in KK221 are located within the boundaries of this isophote, but the location of the brightest cluster and the whole globular cluster system seems to be shifted from the central position in the galaxy. We can only speculate whether KK221 has an elongated orbit and experienced strong tidal forces from NGC5128, which moves its globular cluster system from a centered position.

Globular cluster candidates were selected using the FIND task of the DAOPHOT-II (Stetson 1987) package implemented in MIDAS. The detection threshold was set at  $4\sigma$  above the background. The minimum full width at half maximum input parameter (FWHM) used was  $\sim 0.2''$  (The stellar FWHM is  $\sim 0.15''$ ). Photometry was performed using PHOT task of DAOPHOT-II with a 12 pixel/1.2'' radius. To convert instrumental magnitudes F606W and F814W into the standard Johnson-Cousins system we used the surface photometry recipes and equations presented by Holtzman et al. (1995). Surface brightness profiles and growth curves were computed from the

<sup>2</sup> KK84 is located at a distance of 9.7 Mpc.

**Table 1.** Low surface brightness galaxies in nearby groups and in the field, which were searched for globular cluster candidates. Columns of the table contain the following data: (1) Galaxy Name, (2) equatorial coordinates (J2000), (3) morphological type according to RC3 (de Vaucouleurs et al. 1991), (4) distance in Mpc, (5) integrated absolute  $V$  magnitude (indices refer to 0: this work; K0: Karachentsev et al. (2000); K1a: Karachentsev et al. (2001a); K1b: Karachentsev et al. (2001b); K1c: Karachentsev et al. (2001c); RC3: de Vaucouleurs et al. (1991); M98: Makarova et al. (1998); M99: Makarova (1999)), (6) logarithmic surface gas density of neutral hydrogen in  $M_{\odot}/\text{kpc}^2$ , (7) semi-major axis diameter in kpc, (8) mean surface brightness in  $B$ -band, (9) number of globular cluster candidates, including (10) number of GCCs located outside the isophote of constant surface brightness  $\mu_B = 26.5 \text{ mag/arcsec}^2$ .

Name	RA (2000)	DEC (2000)	T	Dist	$M_V$	$\log\Sigma_{HI}$	$R_{\text{kpc}}$	$SB_{\text{mean}}$	$N_{\text{GCC}}$	$N_{\text{out}}$
<b>M81 group</b>										
KDG52	08 23 56	+71 01 46	10	3.55	-11.71 <sub>0</sub>	7.0	1.3	25.5	0	0
DDO53	08 34 07	+66 10 45	10	3.56	-13.74 <sub>RC3</sub>	7.3	1.7	24.1	1	0
A0952+69	09 57 29	+69 16 20	10	3.87	-11.84 <sub>0</sub>	...	2.0	26.5	0	0
BK3N	09 53 49	+68 58 09	10	4.02	-9.59 <sub>0</sub>	...	0.5	25.6	1	1
KDG73	10 52 55	+69 32 45	10	3.70	-11.31 <sub>0</sub>	7.0	0.6	24.5	1	1
FM1	09 45 10	+68 45 54	-3	3.42	-11.04 <sub>K1c</sub>	...	0.9	25.7	0	0
KK77	09 50 10	+67 30 24	-3	3.48	-12.21 <sub>K1a</sub>	...	2.4	26.4	3	0
KDG61,KK81	09 57 03	+68 35 30	-1	3.60	-13.58 <sub>K1a</sub>	...	2.5	25.4	1	0
KKH57,HS108	10 00 16	+63 11 06	-3	3.93	-10.90 <sub>K1c</sub>	...	0.7	25.3	0	0
KDG63,KK83	10 05 07	+66 33 18	-3	3.50	-12.82 <sub>K1a</sub>	...	1.7	25.5	1	0
KDG64,KK85	10 07 02	+67 49 39	-3	3.70	-13.24 <sub>K1a</sub>	...	2.0	25.1	0	0
DDO78,KK89	10 26 28	+67 39 24	-3	3.72	-12.75 <sub>K1a</sub>	...	2.1	25.8	2	0
BK6N,KK91	10 34 32	+66 00 42	-3	3.85	-11.93 <sub>K1a</sub>	...	1.2	25.5	2	0
Garland	10 03 42	+68 41 36	10	3.7	...	7.3	4.3	...	1	...
Holmberg IX	09 57 32	+69 02 35	10	3.7	-13.8 <sub>0</sub>	7.9	2.5	24.8	14	0
<b>Sculptor group</b>										
E410-005,KK3	00 15 31	-32 10 48	-1	1.92	-12.11 <sub>K0</sub>	...	0.7	24.0	0	0
KDG2,E540-030	00 49 21	-18 04 28	-1	3.40	-12.00 <sub>0</sub>	...	1.2	25.3	1	1
E294-010,PGC1641	00 26 33	-41 51 20	-3	1.92	-11.40 <sub>0</sub>	...	0.6	24.2	1	0
E540-032,FG24	00 50 25	-19 54 25	-3	3.42	-11.84 <sub>0</sub>	...	1.3	25.6	0	0
KK27	03 21 06	-66 19 22	-3	3.98	-12.32 <sub>0</sub>	...	1.4	24.9	1	0
Sc22	00 23 52	-24 42 18	-3	4.21	-11.10 <sub>0</sub>	...	1.1	26.0	3	2
DDO6	00 49 49	-21 00 58	10	3.34	-12.92 <sub>RC3</sub>	6.8	1.7	24.5	0	0
<b>CVn I cloud</b>										
KK166	12 49 13	+35 36 45	-3	4.74	-11.29 <sub>0</sub>	...	1.0	25.2	0	0
DDO113,KDG90	12 14 58	+36 13 08	10	2.86	-12.67 <sub>0</sub>	...	1.2	25.1	2	1
U7605	12 28 39	+35 43 05	10	4.43	-13.88 <sub>M98</sub>	7.3	1.4	23.4	1	0
KK109	11 47 11	+43 40 19	10	4.51	-10.19 <sub>0</sub>	6.9	0.8	25.9	1	1
U7298	12 16 29	+52 13 38	10	4.21	-12.54 <sub>M99</sub>	7.2	1.3	24.5	1	0
U8308,DDO167	13 13 22	+46 19 18	10	4.19	-12.48 <sub>M99</sub>	7.2	1.3	24.0	4	2
U8833	13 54 49	+35 50 15	10	3.19	-12.73 <sub>M98</sub>	7.4	0.8	23.5	0	0
<b>Cent A group</b>										
KK211	13 42 06	-45 12 18	-5	3.58	-12.58 <sub>0</sub>	...	0.8	24.1	2	0
KK213	13 43 36	-43 46 09	-3	3.63	-11.12 <sub>0</sub>	...	0.6	25.5	0	0
KK217	13 46 17	-45 41 05	-3	3.84	-12.18 <sub>0</sub>	...	0.7	24.7	0	0
KK221	13 48 46	-46 59 49	-3	3.98	-11.96 <sub>0</sub>	...	1.7	27.0	5	0
E269-37,KK179	13 03 34	-46 35 03	-3	3.48	-12.57 <sub>0</sub>	...	0.8	24.0	0	0
KK200	13 24 36	-30 58 20	9	4.63	-12.74 <sub>0</sub>	6.6	1.8	25.5	1	0
E444-84	13 37 20	-28 02 46	10	4.61	-13.63 <sub>0</sub>	7.6	1.7	24.0	0	0
<b>N3115 group</b>										
KK84	10 05 34	-07 44 57	-3	9.7	-14.40 <sub>0</sub>	...	4.1	25.4	8	2
<b>Field</b>										
KKR25	16 13 48	+54 22 16	10	1.86	-10.45 <sub>K1b</sub>	6.7	0.6	25.0	0	0
U8508	13 30 44	+54 54 36	10	2.56	-13.42 <sub>M99</sub>	7.3	1.3	23.6	0	0
DDO190,U9240	14 24 44	+44 31 33	10	2.79	-14.37 <sub>RC3</sub>	7.4	1.5	22.9	1	0
E379-07,KK112	11 54 43	-33 33 29	10	5.22	-12.28 <sub>0</sub>	6.9	1.7	25.1	3	0
E321-014	12 13 50	-38 13 53	10	3.19	-13.18 <sub>0</sub>	6.8	1.3	24.0	0	0
KKH5	01 07 33	+51 26 25	10	4.26	-12.64 <sub>0</sub>	7.1	0.7	23.7	0	0
KKH34,Mai13	05 59 41	+73 25 39	10	4.61	-12.70 <sub>0</sub>	6.9	1.2	24.7	0	0
KKH98	23 45 34	+38 43 04	10	2.45	-11.28 <sub>0</sub>	7.1	0.7	25.0	0	0
KK16	01 55 21	+27 57 15	10	4.74	-12.81 <sub>0</sub>	6.7	1.1	23.9	0	0
KK17	02 00 10	+28 49 57	10	4.72	-11.95 <sub>0</sub>	6.7	0.8	24.3	0	0
KKH18	03 03 06	+33 41 40	10	4.43	-12.84 <sub>0</sub>	7.3	0.9	23.8	0	0
E489-56,KK54	06 26 17	-26 15 56	10	4.99	-13.51 <sub>0</sub>	7.4	0.9	22.8	0	0
E490-17,PGC19337	06 37 57	-25 59 59	10	4.23	-14.91 <sub>0</sub>	6.9	2.1	23.5	5	0
U3755	07 13 52	+10 31 19	10	5.22	-15.36 <sub>M99</sub>	6.9	2.6	23.4	32	0
KK65	07 42 31	+16 33 40	10	4.51	-13.32 <sub>0</sub>	7.1	1.2	23.3	1	0
U4115	07 57 02	+14 23 27	10	5.49	-14.12 <sub>0</sub>	7.4	2.9	24.8	3	0
KKH86	13 54 34	+04 14 35	10	2.61	-11.19 <sub>0</sub>	6.6	0.5	24.5	0	0
UA438,E470-18	23 26 28	-32 23 26	10	2.23	-11.94 <sub>0</sub>	7.4	1.0	23.2	2	0
KKH98	23 45 34	+38 43 04	10	2.45	-11.28 <sub>0</sub>	7.1	0.8	25.0	0	0
E321-014	12 13 50	-38 13 53	10	3.19	-13.18 <sub>0</sub>	6.8	1.3	24.0	0	0

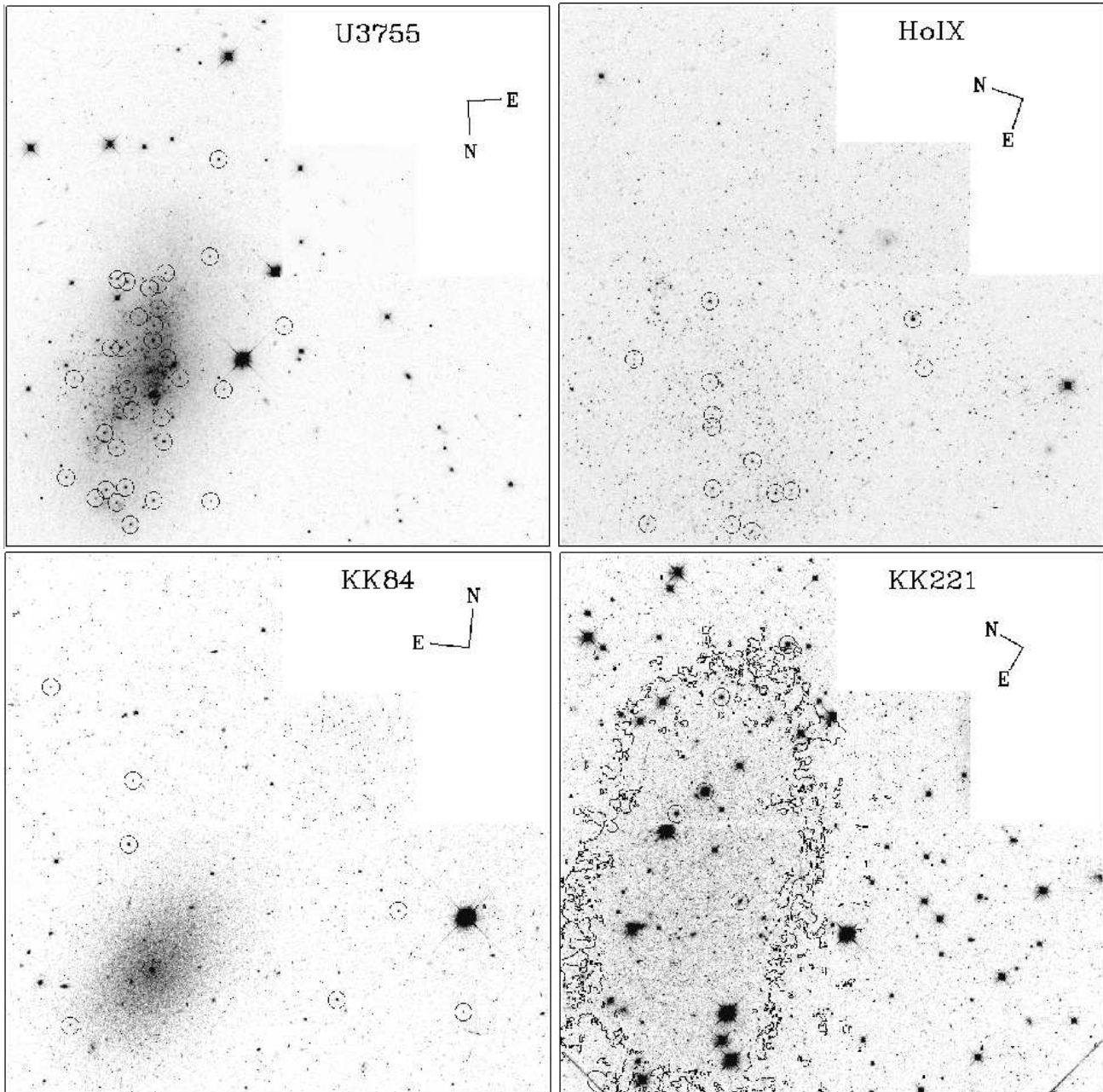


**Fig. 1.** HST/WFPC2 images for U3755, Holmberg IX, KK84, and KK221 which host the richest GCC systems in our sample in their morphology classes (see Section 1 for details).

aperture photometry results. The growth curves were extrapolated to an infinitely large aperture. Finally, the magnitudes of GCCs were corrected for Galactic extinction using reddening maps from Schlegel et al. (1998), and absolute magnitudes were computed by applying the distance moduli reviewed in Karachentsev et al. (2004). Half-light radii and linear projected separations of GCCs from the centers of parent galaxies were converted to a linear measure in parsecs.

We performed photometry of 37 dwarf galaxies using the WFPC2 images and the surface photometry recipes and equations given in Holtzman et al. (1995). All steps were identical to that used in Makarova (1999) and we

refer to this work for further detail. Integrated absolute  $V$  magnitudes are listed in Table 2.

### 3. Cluster Candidate Selection

Our primary target lists include stars, galaxies, and star clusters. In order to select globular cluster candidates we applied a color selection cut of  $0.3 < (V-I)_0 < 1.5$ , which is the full range expected for clusters older than 100 Myr and metallicities  $-2.5 < [Z/Z_\odot] < 0.5$  (e.g. Bruzual & Charlot 2003). We select round objects ( $\text{FWHM}(x) \simeq \text{FWHM}(y)$ ) with half-light radii of  $2 < \text{FWHM} < 9$  pix. Reduced to linear measure in parsecs using the distance measurements

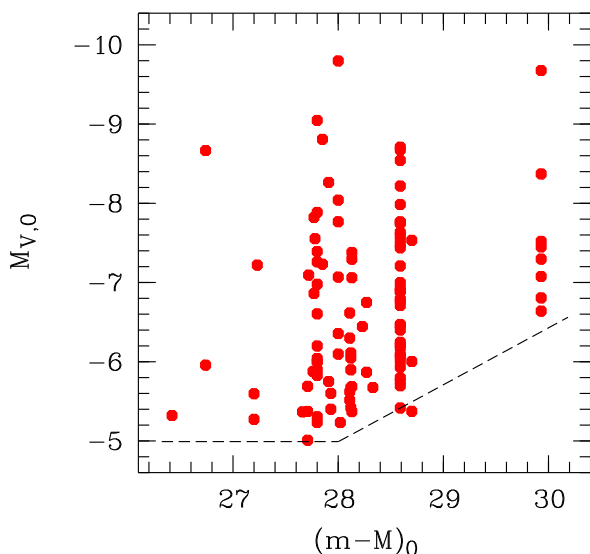


**Fig. 2.** Distance modulus versus absolute  $V$  magnitude for GCCs, identified in this study and listed in Table 2. Our sample is complete down to  $M_V \approx -5$  for all our sample galaxies, except KK84. Detections of GCCs in KK84 are complete down to  $M_V \approx -6.6$  mag.

of Karachentsev et al. (2004), this range corresponds to projected half-light radii  $3 < r_h < 20$  pc, which are within values typical for Galactic globular clusters (Harris 1996, and 2003 update). Then we performed a visual inspection of selected GCCs on the WFPC2 images. The high angular resolution of HST helps us to reject objects which show evidence of spiral or disturbed substructure (most likely background galaxies) from the list of globular cluster candidates.

We apply a lower absolute magnitude limit for our GCCs of  $M_V = -5.0$  mag. For all our images, this magnitude limit is much brighter than the photometric limit of the images ( $V \sim 25.0$  mag), hence no completeness corrections are necessary. In other words, our sample is complete down to  $\sim 2.5$  mag past the presumed turnover of the globular cluster luminosity function (e.g. Harris 2001). Figure 2 shows that GCCs detections for the galaxy KK84 located at a distance of 9.7 Mpc is complete down to  $M_{V,0} \approx -6.6$ . Assuming that globular clusters in this galaxy have an intrinsic luminosity function similar to the Milky Way globular cluster luminosity function, we detect  $\sim 80\%$  of all globular clusters.

Finally, we fit surface brightness profiles to our GCCs with the King law (King 1962)

$$\mu_i = \left( \frac{1}{\sqrt{1+r^2}} - \frac{1}{\sqrt{1+c^2}} \right)^2. \quad (1)$$

We minimize the  $\chi^2$  function:

$$\chi^2 = \sum_i \frac{(\mu_i - \bar{\mu}_i)^2}{\sigma_i^2}, \quad (2)$$

where  $\mu_i$  is an average surface brightness inside a circular ring aperture,  $\bar{\mu}_i$  is the predicted value for the same circular ring, and  $\sigma_i$  is the corresponding photometric error. Nonlinear least-square fits give us the following parameters:  $r_c$  — core radius,  $r_t$  — truncation radius of the King model, concentration parameter  $c = r_t/r_c$ , and  $\mu_0$  — central surface brightness of the GCC. The King law approximation provides us an additional argument to reject background galaxies from our GCCs list. King (1962) emphasized that "relative to globular clusters, giant elliptical galaxies have an excess of brightness near the center". Hence, we rejected objects with a central excess brightness and/or uncertain output parameters. About 10% of the sample was removed in this way by visual inspection. Most of the rejected sources have  $V - I > 1.4$  and are therefore likely to be background galaxies.

The final list of all GCCs in our sample galaxies is presented in Table 2. Parameters obtained by the King-law approximation of GCC surface brightness profiles are listed in the Table 3.

It should be mentioned that, even after applying all our selection procedures, we can not be certain that all objects in our list are genuine globular clusters. Elliptical galaxies at intermediate redshifts are hard to distinguish from globular clusters using  $V$  and  $I$  magnitudes only. Unresolved starbursts with ages  $\leq 300$  Myr at redshifts  $z \sim 0.1 - 1.0$  are potential contaminants (Puzia et al. 2004). We estimate the number of background galaxies down to  $I = 22.5$  mag based on *FORS Deep Field* data (Heidt et al. 2003). We expect  $\sim 3-4$  background galaxies within the WFPC2 field of view with colors resembling those of globular clusters. Eleven of our sample GCCs are located outside the

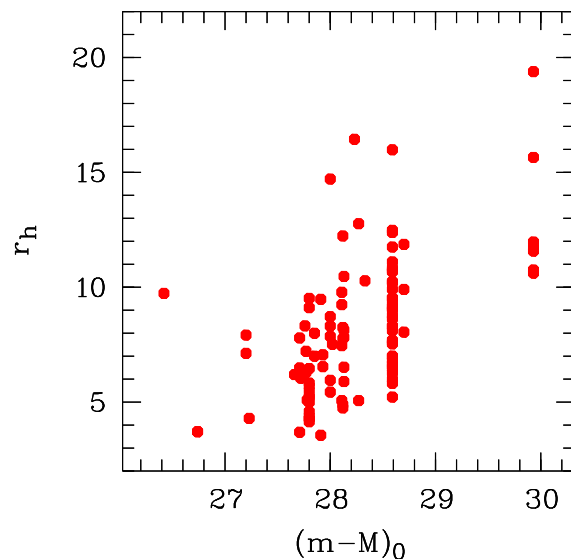


**Fig. 3.** Half-light radius of globular cluster candidates (see Table 3) versus distance modulus of their host galaxies. Our sample is composed mainly of GCCs with core radii  $\sim 3-13$  pc (see Section 3 for details).

$\mu_B \sim 26.5$  mag/arcsec<sup>2</sup> isophotes of their respective host galaxies. The probability that they are background galaxies is higher than for the other GCCs. Five of these GCCs are located in dIrr and dSph/dIrr galaxies and have colors  $(V - I)_0 > 1.2$  and absolute magnitudes within the range  $-5.3 < M_{V_0} < -6.3$ . Another six GCCs are located outside the  $\mu_B \sim 26.5$  mag/arcsec<sup>2</sup> isophote, which have  $0.6 < (V - I)_0 < 1$  and  $-5.2 < M_{V_0} < -6.6$ . Four of these belong to dSphs. Hence, we estimate the contamination of background objects within the boundaries of the  $\mu_B \sim 26.5$  mag/arcsec<sup>2</sup> isophote for our galaxies with  $(V - I)_0 < 1.2$  to be  $\lesssim 10\%$ .

Before analysing properties of GCCs we investigate our sample for observational selection effects. Figure 3 shows the half-light radii of our GCCs (see Table 3) as a function of the distance modulus of their host galaxy. Our sample is mainly composed of GCCs with core radii  $\sim 3 - 13$  pc. With the current dataset we cannot rule out the presence of GCCs fainter than  $M_V \approx -6.5$  and with core radii  $\lesssim 10$  pc in the dSph galaxy KK84, which is the most distant host galaxy in our sample, situated at 9.7 Mpc.

On the other hand, we detect five GCCs with  $r_c > 12$  pc in galaxies that are more distant than 3.8 Mpc. This fact might be caused by two reasons. Firstly, the size of space volume projected into an image pixel increases with increasing of the distance to galaxies. Errors of structural parameters grow accordingly. However, we do not find a significant increase of the mean error for these five objects compared to the rest of our sample. Secondly, the surveyed area of galaxies grows with distance. This might lead to a higher detection rate of large GCCs in the outskirts of these galaxies. Two of these five objects are located at the largest galactocentric radii with respect to their host galaxy (see Section 5 for details). This in turn means that we might miss a few extended globular cluster candidates in nearby galaxies at large galactocentric radii. Larger field coverage for nearby systems would help to resolve this issue. For the remainder of this work, we keep in mind that the lack of extended GCCs in nearby galaxies is a potential bias of our current dataset.

## 4. Properties of Globular Cluster Candidates

### 4.1. Colors

Figure 4 shows a color-magnitude diagram for all GCCs. Colors and magnitudes were corrected for Galactic foreground extinction using the reddening maps of Schlegel et al. (1998). We have no means to correct for internal reddening of the observed dIrr galaxies. However, given the similarity of these systems to nearby dIrr galaxies we estimate that this correction is  $E_{(B-V)} \lesssim 0.1$  mag (James et al. 2005). Hence, we refer in the following to foreground extinction corrected magnitudes and colors by indexing them with a zero.

A KMM test (Ashman et al. 1994) for GCCs in dIrrs returns peaks at  $(V - I)_0 = 0.48 \pm 0.02$  and  $1.02 \pm 0.03$  mag with dispersions 0.12 and 0.22 mag for the blue and

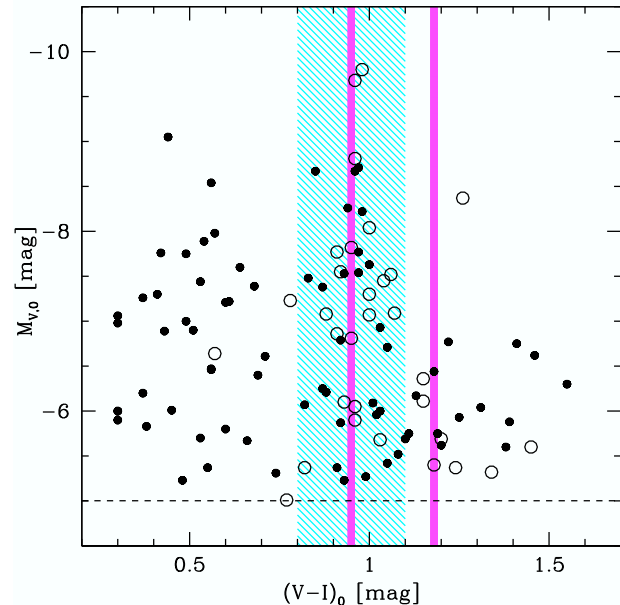


**Fig. 4.** Color-magnitude diagram of globular cluster candidates in dSph (*open circles*) and dIrr galaxies (*solid dots*), identified in this study and listed in Table 2. The dashed line indicates the limit of our photometry (see Sect. 3 for details). Note that there are virtually no GCCs in dSph galaxies with colors bluer than  $(V - I)_0 \approx 0.7$  mag. The hatched region shows the color range where most Galactic and M31 globular clusters are found (see Puzia et al. 2004). The two vertical lines indicate colors of blue and red sub-populations in massive early-type galaxies (e.g. Kundu & Whitmore 2001a,b; Larsen et al. 2001).

red peak, respectively. The peak of the dSph distribution is located at  $(V - I)_0 = 1.01 \pm 0.03$  mag and has a dispersion of 0.18 mag. The red peak GCC sub-population in dIrrs and most GCCs in dSph galaxies cover the same  $(V - I)_0$  color range as the ancient Galactic and M31 globular clusters (see Fig. 1 in Puzia et al. 2004). More than  $\sim 50\%$  of all globular cluster systems in massive early-type galaxies show indications for multi-modality, with mean peak colors at  $(V - I)_0 \approx 0.95$  and  $\sim 1.18$  mag (e.g. Kundu & Whitmore 2001a,b; Larsen et al. 2001). So far most of these globular cluster systems were found to be old (Puzia et al. 1999; Jordán et al. 2002). A comparison of  $(V - I)_0$  colors reveals that most GCCs in dSphs and the red-peak GCCs in dIrrs are similar to *blue* globular clusters in early-type galaxies (see vertical lines in Fig. 4), which implies similar ages and metallicities. The blue sub-population of GCCs in dIrr galaxies is significantly bluer and suggests much younger ages and/or lower metallicities.

Figure 5 shows the color histogram for GCCs in dIrr and dSph galaxies. The distribution of  $(V - I)_0$  colors exhibits an obvious bimodality for GCCs in dIrr galaxies, in contrast to the distribution of GCCs in dSph galaxies, which shows a single mode distribution. The clear differ-



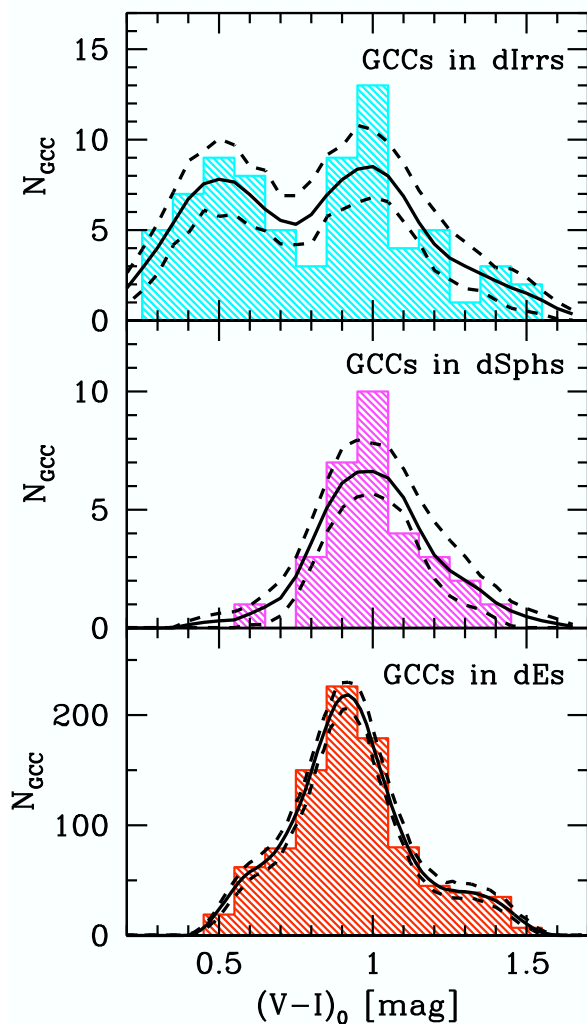


**Fig. 5.** Color distributions of globular cluster candidates in dSph, dIrr, and dE galaxies. The upper and middle panel show our data, while the bottom histogram was constructed from data taken from Lotz et al. (2004). Solid lines indicate a non-parametric probability density estimate using an Epanechnikov kernel (Silverman 1986). Dashed lines show 90% confidence limits.

ence between the two distributions is underlined by a non-parametric probability density estimate (Silverman 1986). The color of the red peak in the dIrr distribution is virtually identical with the mean of the dSph distribution. Their dispersions are also very similar. This points to the fact that both galaxy types host similar globular cluster populations.

We compare the color distributions of GCCs in dIrr and dSphs with that of dE galaxies. In the bottom panel of Figure 5 we present the color histogram of globular cluster candidates in 69 dwarf elliptical galaxies in the Virgo and Fornax galaxy clusters and the Leo group, with data taken from Lotz et al. (2004). The peak of this distribution is at  $(V-I)_0 = 0.90 \pm 0.03$  mag. The dE color distribution, in particular the red end, is similar to the one of dSph GCCs

and the red peak of the dIrr distribution. It is remarkable that the dE color distribution is shifted to bluer colors by  $\sim 0.1$  mag with respect to the mean color of the dSph and the red peak of the dIrr GCC sub-population. This indicates a mean difference in age and/or metallicity. To better assess the reality of this color difference, we carried out an independent photometry of GCCs in one galaxy (VCC1254) from the sample of Lotz et al. (2004). For this purpose we applied our photometric routines to the identical images as used in the Lotz et al. study and compared our results to their work. We found a small systematic offset  $\Delta(V-I) = 0.04 \pm 0.05$  for 21 common objects, in the sense that our values tend to be redder. This indicates that different photometric approaches might have a small influence on our conclusions. A Kolmogorov-Smirnov test shows that there is a 0.03% likelihood that the dE and dSph color distributions were drawn from the same sample. This likelihood decreases significantly for the other combinations dE-dIrr and dSph-dIrr.

SSP models (e.g. Bruzual & Charlot 2003) predict that for a solar-metallicity, 13 Gyr old stellar population a  $\Delta(V-I)_0 = 0.1$  difference translates into  $\sim 7$  Gyr younger ages (at the same metallicity) and/or a  $\sim 0.6$  dex smaller metallicity (at the same age). Because of the age-metallicity degeneracy of photometric colors, it is difficult to derive individual ages and metallicities from two colors only. However, a comparison of the colors with current SSP models shows that  $(V-I) \approx 1.0$  mag is consistent with stellar populations with a certain combination of ages older than 1 Gyr and metallicities  $[Z/H] \gtrsim -1.4$  dex. The blue peak of the dIrr color distribution, on the other hand, is consistent with stellar populations that have ages  $\lesssim 1$  Gyr and metallicities  $[Z/H] \gtrsim -2.0$  dex. Thus, we suggest that red-peak GCCs in dIrr and most GCCs in dSph are metal-rich globular clusters with intermediate to old ages. Blue GCCs in dIrr galaxies are likely to be relatively young globular clusters, probably similar to populous star clusters found in several star-forming nearby galaxies (e.g. Larsen & Richtler 2000).

#### 4.2. Luminosity Function

In addition to a blue and likely younger population of GCCs in dIrrs, the color distributions revealed a red and presumably ancient population in both dSph and dIrr galaxies. To investigate the luminosity functions (LFs) of these sub-populations individually, we split the dIrr sample at  $(V-I)_0 = 0.75$  mag (see Fig. 5) into red and blue cluster candidates. The corresponding LFs are shown in Figure 6 down to  $\sim 2.5$  mag past the turnover of a typical globular cluster luminosity function, which is indicated by a vertical line (Harris 2001).

The LF of blue GCCs seems broad with a turnover somewhere between  $M_V \approx -7.5$  and  $-6.0$  mag. The fact that we see a turnover for these supposedly young clusters is remarkable, since constant power-law slopes down to faint magnitudes are observed in other globular

cluster systems of similar age (e.g. Whitmore et al. 1999; Goudfrooij et al. 2004). While these clusters are found in dense environments of ongoing mergers and massive early-type galaxies, our sample GCCs are located in low-mass galaxies in loose groups and the field. The reason that we see a turnover in a young cluster system might be a consequence of fundamentally different mechanisms of star cluster formation. The star formation rate in our sample dIrrs is relatively low. Hence, slow spontaneous instabilities are likely to dominate the star formation process, that do not support the formation of gravitationally bound low-mass star clusters. Another possible explanation might be more efficient destruction processes, such as infant mortality (Lada & Lada 2003), which is thought to be the consequence of early gas ejection. In general, since physical differences between young star clusters are related to the pressure differences of the environment in which they form (e.g. Elmegreen & Efremov 1997; Ashman & Zepf 2001), slight differences in luminosity functions of young globular cluster systems in different environments cannot be excluded.

The LF of red GCCs in dIrrs turns over at a much fainter magnitude  $M_V \approx -6$  mag than for their blue counterparts. We can only speculate whether this is due to a difference in formation mechanisms, ages/metallicities, or simply due to contamination by background galaxies. We point out that contamination by stellar crowding is more likely to occur in dIrr galaxies, which are populated by bright stars. However, stellar crowding is unlikely to explain the excess of objects, which is also found in dSph galaxies (see below).

For GCCs in dSphs the luminosity function shows a turnover at around  $M_V = -7.4$  mag. Similar turnover magnitudes are also found in many other globular cluster systems (Harris 2001). In addition to a roughly log-normal LF for bright objects, we find that the luminosity functions of GCCs fainter than  $M_V = -6.5$  mag are steadily increasing towards fainter magnitudes, possibly resembling a dynamically less evolved population of clusters (Gnedin & Ostriker 1997; Fall & Zhang 2001). The existence of an excess population of faint globular cluster candidates in dSphs is surprising and is reported on here for the first time. A scaled *Student*  $t_5$ -distribution

$$t_5(m|M_{V,0}, \sigma_t) = \frac{8}{3\pi\sigma_t\sqrt{5}} \left( 1 + \frac{(m - M_{V,0})^2}{5\sigma_t^2} \right)^{-3}, \quad (3)$$

that is the best approximation to the observed Galactic globular cluster luminosity function (Secker 1992, see dashed line in the bottom panel of Fig. 6), shows good agreement with the bright peak<sup>3</sup>, where  $M_{V,0} = -7.4$  and  $\sigma_t = 0.6$ . The faint cluster excess can be well approximated by a second  $t_5$ -peak with a mean at  $M_{V,0} \approx -5.2$  mag and roughly twice as broad a dispersion as the bright peak. This is reminiscent of the composite luminosity function of globular and open clusters in the Milky Way.

<sup>3</sup> This approximation neglects two very bright GCCs with magnitudes  $M_V \approx -10$ .

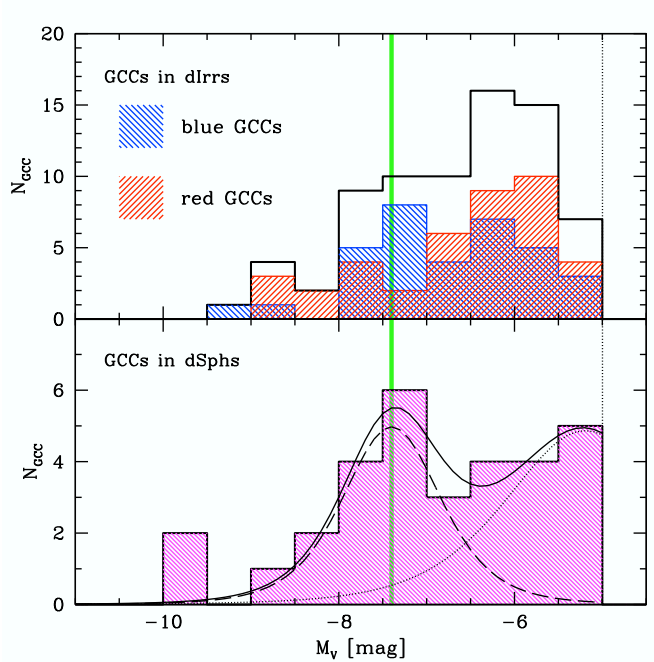


**Fig. 6.** Luminosity functions of globular cluster candidates in dIrr (*top panel*) and dSph galaxies (*bottom panel*). The luminosity function of red and blue GCCs in dIrr galaxies are also shown in as hatched histograms. The shaded vertical line indicates the turnover of the Galactic globular cluster luminosity function. The dotted line represents our photometric limit.

However, since this is a composite luminosity function for GCCs in different galaxies, various dynamical processes are lumped together in one sample. This and the possibility of variable internal reddening might account for at least part of the spread in the observed luminosity function.

We note that a similar excess population of faint star clusters has been discovered in the low-mass spiral M33 (Chandar et al. 2001) and in nearby lenticular galaxies (Brodie & Larsen 2002). However, the nature of these faint excess clusters is difficult to assess based on two-color photometry. Bright nuclei of barely resolved background galaxies might contribute to the faint GCC excess.

For KK84 and UGC 3755, which host the richest GCC systems in their morphology class, we investigate their GCC luminosity distributions individually. The GCC luminosity function of the dSph galaxy KK84 peaks near  $M_V \approx -7.3$  mag. For the dIrr galaxy UGC 3755 we find peaks near  $M_V \approx -7.0$  mag for both the blue and red sub-population. Both galaxies are relatively massive compared to the rest of the sample and show typical turnover magnitudes.

In summary, given the number statistics of our data, we can say that, compared to a typical globular cluster luminosity function, both the dSph and dIrr GCC populations exhibit an excess of faint globular cluster candidates. Whether this is due to a genuine new population of low-



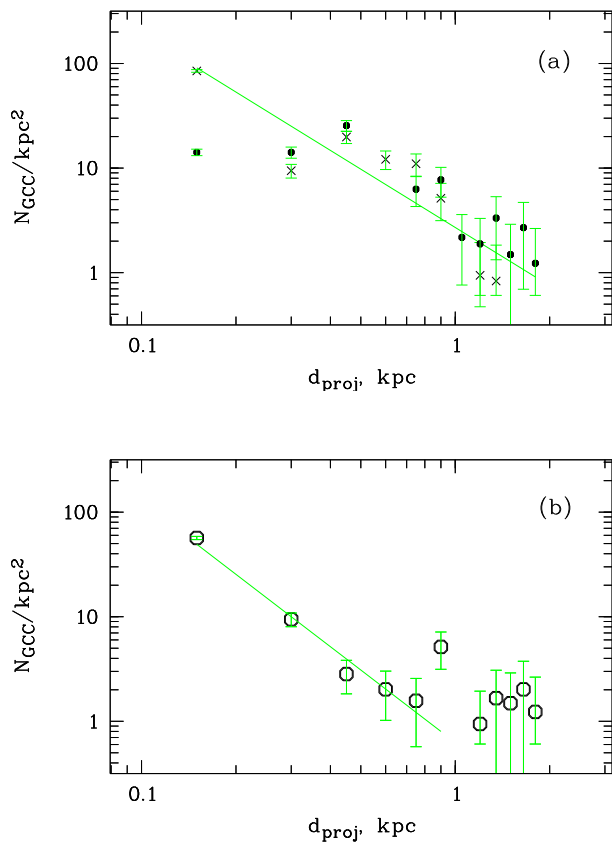


**Fig. 7.** Radial distribution of GCCs in dIrr galaxies (*panel a*) and dSph galaxies (*panel b*). The sample of GCCs in dIrrs is divided into blue GCCs with  $(V - I)_0 < 0.75$  (*dots*) and red GCCs  $(V - I)_0 > 0.75$  (*crosses*). Plotted here is the logarithm of the surface density of GCCs per square kpc (evaluated in 0.15-kpc bins) vs. the logarithmic projected distance from the galaxy center, in kpc.

mass star clusters or due to contamination by marginally resolved background galaxies will be resolved with spectroscopic data.

### 4.3. Spatial Distributions

In the following, we compare the composite spatial distribution of GCCs in dSph and dIrr galaxies. We divide the population of GCCs in dIrr galaxies into red and blue objects at  $(V - I)_0 = 0.75$  mag. In Figure 7 we plot the logarithmic number density of GCCs per square kpc versus the logarithm of the linear projected separation from the galaxy center in kpc, for dIrr and dSph galaxies. Radial distributions of blue and red GCCs in dIrrs are shown by different symbols and reveal somewhat different slopes. A power law for the surface density of the form  $\rho = r^{-x}$  gives a good fit to our data. We find that the surface density profiles of globular cluster systems in dIrr galaxies are “flatter” ( $x_{\text{red}} \approx 1.1$ ) and ( $x_{\text{blue}} \approx 1.85$ ) than those in dSph galaxies ( $x \approx 2$ ). The profile for GCCs in dSph

galaxies seems to flatten out beyond  $\sim 1$  kpc galactocentric distance. Hence, the fit includes only the inner part of the GCC population. The profiles of the GCC population in dIrr galaxies do not show a flattening at large galactocentric distances.

These values are in good agreement with those found for globular cluster systems in elliptical ( $x = 0.8 - 2.6$ , Puzia et al. 2004) and dwarf elliptical galaxies ( $x = 1.6 \pm 0.4$ , Durrell et al. 1996). Moreover, Harris (1986) found  $x = 3.5 \pm 0.5$  for the combined spatial distribution of globular clusters in NGC 147, NGC 185 and NGC 205. Minniti et al. (1996) constructed a composite dwarf elliptical galaxy from all early-type dwarf galaxies in the Local Group and computed  $x = 2.1$ .

### 4.4. Structural Parameters

Under the superb spatial resolution of HST/WFPC2, typical globular clusters (Harris 1996) begin to be resolved for galaxies less distant than  $D \sim 10$  Mpc. Using our King-profile approximation routine we measure structural parameters for all our sample GCCs. Figure 8 shows half-light radii,  $r_h$ , and core radii,  $r_c$  of GCCs as a function of their projected galactocentric distance. Both panels show a trend of increasing half-light and core radius as a function of increasing galactocentric distance. These correlations are however driven by the outermost GCCs. Spectroscopy is necessary to measure their radial velocities and test whether these objects are genuine globular clusters or resolved background galaxies. If we consider GCCs with projected distances less than  $\sim 1$  kpc to avoid potential contamination by background sources (see Fig. 7b), we find only tentative evidence for a  $r_c - d_{\text{proj}}$  correlation. With the same radial constraint we find no correlation between half-light radius and galactocentric distance.

Such correlations exist for half-light radii and core radii of Galactic and Large Magellanic Cloud (LMC) globular clusters (van den Bergh 2000; de Grijs et al. 2002; van den Bergh & Mackey 2004). We find that at a given galactocentric distance our sample GCCs have on average a factor of  $\sim 5$  larger half-light radii than LMC globular clusters. This might be due to the higher mass of LMC, which has a stronger tidal field in which destruction processes are enhanced compared to our sample dIrr galaxies. The current dataset reveals no difference between the average structural parameter distribution of GCCs in dIrr and dSph galaxies.

We detect two GCCs in dSph galaxies at small galactocentric radii with structural parameters significantly larger than what one would expect from the extrapolation of the remaining sample. These clusters might be fainter analogues of nuclear star clusters found in dwarf elliptical galaxies (Durrell et al. 1996), that spiraled into the cores of their host galaxies through the process of dynamical friction and orbital decay (Lotz et al. 2001). These two GCCs are among the brightest objects in our sample ( $M_V = -9.7$  and  $-7.8$  mag, see Tab. 2), but they are sig-

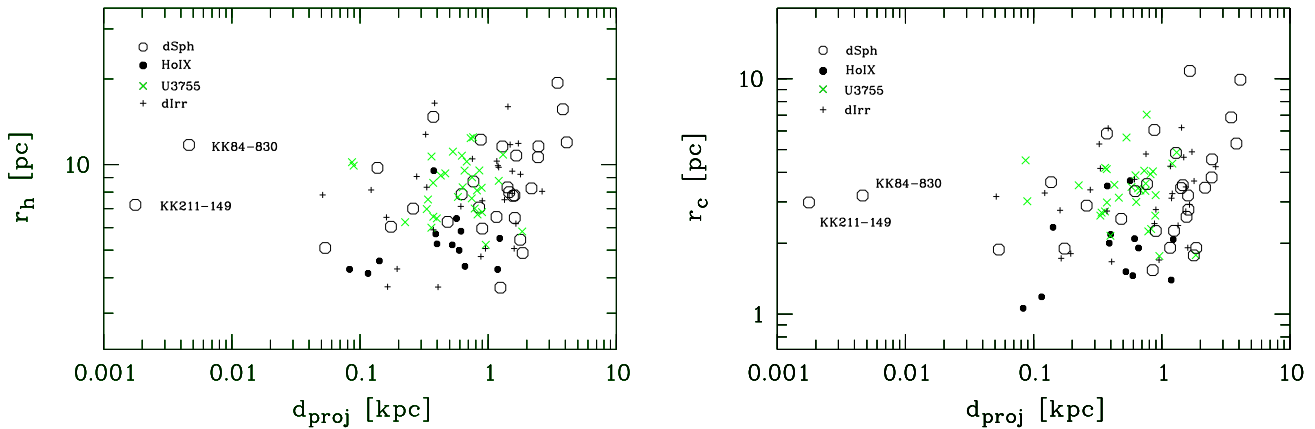


**Fig. 8.** *Left panel:* Half-light radius of our sample GCCs versus their projected galactocentric distance. *Right panel:* Core radius of GCCs versus their projected galactocentric distances. The data for the two richest GCC systems, the dIrr galaxies UGC 3755 and Holmberg IX, are marked by different symbols.

nificantly larger and fainter than nuclear star clusters in late-type spiral galaxies, which have typical sizes between  $r_h \approx 2$  and 10 pc and magnitudes between  $M_V \approx -10$  and  $-13$  mag (Böker et al. 2004). These two nuclear GCCs are also much smaller than the cores of ultra-compact dwarf galaxies, which were recently discovered in the Fornax galaxy cluster (Hilker et al. 1999; Drinkwater et al. 2003).

We also consider structural parameters of the newly discovered population of faint and extended star cluster in lenticular galaxies, termed “faint fuzzies” (Brodie & Larsen 2002), which have typical half-light radii  $r_h > 7$  pc and magnitudes fainter than  $M_V = -7.5$  (see Figure 9). In fact we find that roughly half of our sample is consistent with their magnitudes and structural parameters. The colors of these “faint fuzzy” clusters are around  $(V - I)_0 \approx 1.3$ . We find several faint and extended GCCs in our sample with very similar colors. However, the majority is bluer and has colors typical of the red sub-population with a mean at  $(V - I)_0 \approx 1.0$  mag. We note that the most extended globular clusters in the Local Group spirals and the Magellanic Clouds resemble these faint fuzzies as well.

Figure 9 shows the distribution of our GCCs in the half-light radius versus luminosity plane. A large fraction of GCCs exhibits luminosities and half-light radii consistent with “faint fuzzy” star clusters. The majority of GCCs, however, fall below the relation found by van den Bergh & Mackey (2004), where almost all of the Galactic globular clusters reside. Moreover, the figure shows that some GCCs, primarily those in dSph galaxies, show luminosities and structural parameters similar to those found for NGC 2419 and  $\omega$ Cen, two atypically extended Galactic halo globular clusters (van den Bergh & Mackey 2004).

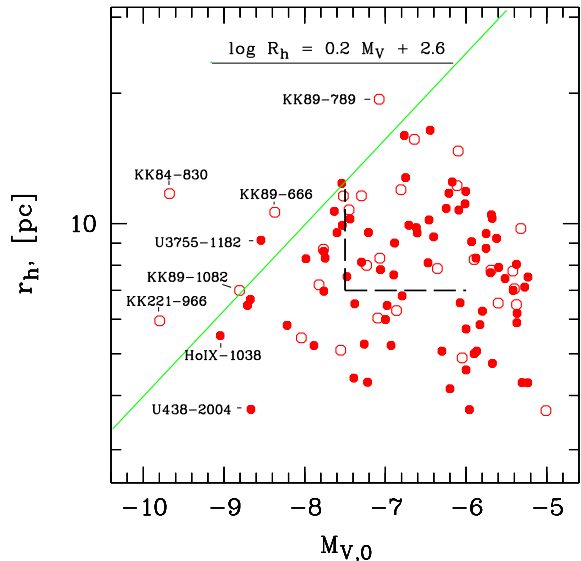


**Fig. 9.** Half-light radii of GCCs in dSph (*open circles*) and dIrr galaxies (*solid dots*) versus their luminosities,  $M_{V,0}$ . The figure shows that almost all GCCs lie below the relation for Galactic globular clusters (*solid line*, see van den Bergh & Mackey 2004), except some GCC in dSphs and one GCC in UGC3755. The most interesting cases of bright and compact GCCs in dIrrs and bright and diffuse GCCs in dSphs are labeled. Roughly half of GCCs is consistent with luminosities and structural parameters of the “faint fuzzies” of Brodie & Larsen (2002), whose location is indicated by two dashed lines ( $M_V > -7.5$  and  $r_h > 7$  pc).

#### 4.5. Compact Star Clusters in Holmberg IX?

We find that GCCs in the dIrr galaxy Holmberg IX are on average more compact than those situated in dSph and

other dIrr galaxies (see Fig. 8). Almost all Holmberg IX GCCs are blue with a mean  $(V-I)_0 = 0.45 \pm 0.16$  and are likely to be young ( $t \lesssim 1$  Gyr). The youth of these clusters could be the reason for their compactness, as either cluster destruction processes did not have enough time to significantly alter their sizes and/or the initial conditions during cluster formation in Holmberg IX were different from those in other galaxies, for instance due to significantly higher ambient pressure.

In a study of structural parameters of LMC globular clusters, de Grijs et al. (2002) found that older clusters exhibit a much greater spread in core radii than their younger counterparts. If the increased spread is due to advanced dynamical evolution, one would expect a smaller spread in sizes of old globular clusters in less massive galaxies. We will test this hypothesis once accurate spectroscopic ages and chemical compositions become available.

## 5. Discussion

### 5.1. Extended Globular Clusters

There is increasing evidence in the current literature that low-mass galaxies host a significant population of faint and extended globular clusters. M33 is the most prominent example (Chandar et al. 2001, 2004). Different physical mechanisms tend to destroy clusters with time: evaporation, disk shocking, tidal shock heating, dynamical friction etc. (e.g. Gnedin & Ostriker 1997; Surdin & Arhipova 1998; Fall & Zhang 2001). The efficiency of tidal disruption increases significantly with the presence of a bulge component (Gnedin & Ostriker 1997). M33 as well as the dwarf galaxies in our sample have no significant bulge component and faint and extended globular clusters are able to survive significantly longer than in the Milky Way or M31. Consequently, there are no indications for an excess population of faint and extended globular clusters in the Milky Way or the inner halo of M31 (Harris 2001; Barmby et al. 2001; van den Bergh & Mackey 2004), as the efficiency of cluster disruption steeply drops with galactocentric distance.

If accretion of globular clusters plays an important role in the assembly of outer globular cluster systems in massive galaxies, one should expect similarities in magnitudes and structural parameters between clusters in our sample dwarf galaxies and the outskirts of the Local Group spirals. Indeed, most of our GCCs have similar structural parameters and luminosities as the most extended Galactic and M31 globular clusters, which are located at large galactocentric distances. This hints at the accretion of such extended clusters from satellite dwarf galaxies (see also Forbes et al. 2004). However, most of the outer halo Galactic globular clusters are metal-poor ( $[Z/H] \lesssim -1$ ) and old ( $t \gtrsim 10$  Gyr). If the accretion scenario for the outer-halo Galactic globular clusters is correct, then they must have formed early, perhaps in Searle-Zinn-type proto-galactic clumps (see Searle & Zinn 1978).

It was recently found that the chemical composition of LMC globular clusters is not entirely reflected in the globular cluster systems of Local Group spirals (e.g. Puzia et al. 2005). Hence, the scenario of the assembly of their outer-halo globular cluster systems by accretion of LMC-type globular clusters seems less likely. A detailed spectroscopic investigation of globular clusters in dwarf galaxies will certainly help to constrain the picture of globular cluster accretion from satellite dwarf galaxies, and will also provide insight into the assembly history of globular cluster systems in giant elliptical galaxies.

### 5.2. Star Clusters in Dwarf Galaxies

Our sample consists of the lowest-mass nearby dwarf galaxies and is representative and homogeneous enough to study the presence of GCCs as a function of general galaxy properties, such as morphological type. The faintest galaxies in our sample are dSphs, with mean surface brightnesses as faint as  $\mu_B \approx 24.4$  mag/arcsec<sup>2</sup> (see Tab. 2). Roughly half of our dIrr galaxies are in the same magnitude range. The detection rate of GCCs in these faint dIrr is  $\sim 2$  times lower than in dSphs (and the other higher surface brightness dIrrs). Only 5 out of 19 faint dIrr galaxies contain GCCs, whereas 10 of 18 dSphs harbor GCCs, at similar host galaxy luminosities. It is not known what causes this discrepancy. We speculate that dSph galaxies turned their gas reservoir earlier and more efficiently into stars than dIrr galaxies of similar luminosity. This was perhaps due to a higher virial density (from stars, gas and dark matter) and higher ambient pressure in the early environments of dSph galaxies. Another reason might be the different stellar  $M/L$  ratio in dSph and dIrr.

It should be mentioned, that our sample dSphs reveal an outstanding feature: in contrast to dIrr galaxies,  $\sim 60\%$  of dSphs with GCCs have cluster candidates located near their galaxy center. These GCCs are bright and compact ( $-7 < M_{V,0} < -10$ ,  $r_c \approx 2 - 3$  pc), similar to those found at the center of nucleated Virgo dEs (Lotz et al. 2004).

It was shown in Section 4.3, that the surface density profiles of globular cluster systems in dSph galaxies are steeper than those in dIrrs. In general, we find that GCC systems of dSph galaxies are more spatially concentrated than in dIrr galaxies. The red sub-population of GCCs in dIrrs shows the "flattest" profile. Blue GCCs in dIrr galaxies, on the other hand, have the tendency to reside in central regions of their host galaxies, but they are still less concentrated than GCCs in dSphs. This difference implies that globular cluster formation and/or evolution histories in both galaxy types were spatially not alike. Globular clusters presumably form where gas is undergoing agitated star formation. With respect to star formation histories, both dSphs and dIrrs appear to be inhomogeneous classes of galaxies (e.g. Mateo 1998). The difference in GCC surface density profiles might reflect a bias of powerful star formation events towards the center of dSph and/or more

efficient orbital decay of star clusters in these galaxies (e.g. Lotz et al. 2001).

Both the dIrr and dSph galaxies share a sub-population of red globular clusters with very similar mean  $(V - I)_0$  colors. In addition to this GCC population, dIrr galaxies host a very blue population of clusters, that are likely to be younger. The bimodality of the GCC color distribution in dIrr galaxies implies two different episodes and/or mechanisms of cluster formation. Similar GCC colors as in dSphs are found for GCCs in dE galaxies (see Sect. 4.1). There is however a very puzzling offset of  $\Delta(V - I)_0 \approx 0.1$  between GCCs in dE and dSph galaxies, where GCCs in dE are bluer. This can be interpreted as the result of lower metallicities and/or younger ages.

The question for the reason of this age and/or metallicity difference is difficult to answer. However, one can consider the globular cluster system of the Fornax dSph galaxy in the Local group as a first reference to learn more about ages and metallicities of field and cluster stellar populations. Red giant branches of all globular clusters in Fornax dSph show steeper slopes than the mean RGB slope of the field stellar population (e.g. Buonanno et al. 1998, 1999). Using RGBs of Galactic globular clusters as reference, all globular clusters in Fornax dSph were found to have low metallicities. This was confirmed by a spectroscopic study of their integrated-light (Strader et al. 2003), which found a mean metallicity of  $[\text{Fe}/\text{H}] \approx -1.8$  and old ages. First attempts to obtain spectroscopic age and metallicity estimates for globular clusters in dEs are on the way (Miller et al. 2004).

From a study of surface brightness fluctuations, Jerjen et al. (2004) showed that Virgo dE galaxies follow a galaxy metallicity–luminosity relation. Virgo dEs should therefore be expected to have on average  $\sim 0.7$  dex higher metallicities compared to the 100 times fainter LG dSph galaxies. Assuming old ages for their GCCs in dEs, Lotz et al. (2004) find a correlation between the mean globular cluster color and host galaxy luminosity, which implies a globular cluster metallicity-galaxy luminosity relation of the form  $\langle Z_{\text{GCC}} \rangle \propto L_B^{0.22 \pm 0.05}$ . This relation implies bluer globular clusters colors in fainter galaxies. Globular clusters have generally bluer colors than their host galaxies (Ashman & Zepf 1998), and the two relations suggest that this offset is present at all galaxy luminosities. According to those relations, globular clusters in dEs are expected to have higher metallicities than in dSph galaxies. Therefore, *younger ages* might be responsible for the bluer colors of globular clusters in dE galaxies.

It is important to continue the study of globular cluster systems in nearby low-mass galaxies and to compare their properties as a function of different host galaxy properties, e.g. morphological type and environmental density.

*Acknowledgements.* MES and DIM are partially supported by a RFBR 04-02-16115 grant. THP is supported by an ESA Research Fellowship, which is gratefully acknowledged. DIM thanks the Russian Science Support Foundation. MES kindly thanks I.D. Karachentsev for initiating the beginning of a work

on searches of globular clusters in dSph galaxies and Vladimir Surdin for useful discussions. We thank Jennifer Lotz for providing data of globular cluster candidates in dwarf elliptical galaxies in electronic form. THP thanks Rupali Chandar, Nicole Homeier, and Jennifer Lotz for useful discussions. We thank the anonymous referee for helpful comments.

## References

- Ashman, K. A., Bird, C. M., & Zepf, S. E. 1994, *AJ*, 108, 2348  
 Ashman, K. M. & Zepf, S. E. 1998, *Globular cluster systems*, Cambridge, U. K. ; New York : Cambridge University Press  
 Ashman, K. M., & Zepf, S. E. 2001, *AJ*, 122, 1888  
 Barmby, P., Huchra, J. P., & Brodie, J. P. 2001, *AJ*, 121, 1482  
 Billett, O. H., Hunter, D. A., & Elmegreen, B. G. 2002, *AJ*, 123, 1454  
 Böker, T., Sarzi, M., McLaughlin, D. E., van der Marel, R. P., Rix, H., Ho, L. C., & Shields, J. C. 2004, *AJ*, 127, 105  
 Bothun, G., Impey, C., & McGaugh, S. 1997, *PASP*, 109, 745  
 Boyce, P. J., et al. 2001, *ApJL*, 560, L127  
 Brodie, J. P., & Larsen, S. S. 2002, *AJ*, 124, 1410  
 Bruzual, G. & Charlot, S. 2003, *MNRAS*, 344, 1000  
 Buonanno, R., Corsi, C., Fusi Pecci, F., & Zinn, R. 1999, *AJ*, 118, 1671  
 Buonanno, R., Corsi, C., Zinn, R., Fusi Pecci, F., Hardy, E., & Suntzeff, N. 1998, *ApJ* 501, L33  
 Chandar, R., Bianchi, L., & Ford, H. C. 2001, *A&A*, 366, 498  
 Chandar, R., Whitmore, B., & Lee, M. G. 2004, *ApJ*, 611, 220  
 de Grijs R., Gilmore, G.F., Mackey, A.D. et al. 2002, *MNRAS*, 337, 597  
 Davies, J. I. & Phillipps, S. 1988, *MNRAS*, 233, 553  
 Drinkwater, M. J., Gregg, M. D., Hilker, M., Bekki, K., Couch, W. J., Ferguson, H. C., Jones, J. B., & Phillipps, S. 2003, *Nature*, 423, 519  
 Durrell, P. R., Harris, W. E., Geisler, D., & Pudritz, R. E. 1996, *AJ*, 112, 972  
 Elmegreen, B. G. & Efremov, Y. N. 1997, *ApJ*, 480, 235  
 Elmegreen, B. G. 2002, *ApJ*, 577, 206  
 Fall, S. M., & Zhang, Q. 2001, *ApJ*, 561, 751  
 Ferguson, H. C. & Binggeli, B. 1994, *A&ARv*, 6, 67  
 Forbes, D. A., Strader, J., & Brodie, J. P. 2004, *AJ*, 127, 3394  
 Gnedin, O. Y., & Ostriker, J. P. 1997, *ApJ*, 474, 223  
 Goudfrooij, P., Gilmore, D., Whitmore, B. C., & Schweizer, F. 2004, *ApJL*, 613, L121  
 Heidt, J., et al. 2003, *A&A*, 398, 49  
 Harris, W. E. 1986, *AJ*, 91, 822  
 Harris, W.E. 1996, *AJ*, 112, 1487, for the 2003 update see <http://physun.physics.mcmaster.ca/~harris/mwgc.dat>  
 Harris, W. E. 2001, *Saas-Fee Advanced Course 28: Star Clusters*, 223  
 Hilker, M., Infante, L., Vieira, G., Kissler-Patig, M., & Richtler, T. 1999, *A&AS*, 134, 75  
 Hodge, P. W., Skelton, B. P., & Ashizawa, J. 2002, *An Atlas of Local Group Galaxies*. By Paul. W. Hodge, Brooke P. Skelton, Joy Ashizawa. University of Washington, Astronomy Department, Seattle, U.S.A. Astrophysics and Space Science Library, Volume 221. Kluwer Academic Publishers, Dordrecht, 2002  
 Holtzman, J. A., Burrows, C. J., Casertano, S., Hester, J. J., Trauger, J. T., Watson, A. M., & Worthey, G. 1995, *PASP*, 107, 1065  
 Hunter, D. A. & Elmegreen, B. G. 2004, *AJ*, 128, 2170  
 Impey, C. & Bothun, G. 1997, *ARA&A*, 35, 267

**Table 2.** List of globular cluster candidates (GCCs) in nearby LSB dwarf galaxies. The columns contain the following data: Identifier of each cluster, composed of the (name of its host galaxy)-(WFPC2 chip)-(cluster numbering), X, Y coordinates derived from the WFPC2 frames, equatorial coordinates (J2000.0), half-light radius  $r_h$  in parsecs, apparent axial ratio  $e = 1 - b/a$ , integrated absolute  $V$  magnitude (corrected for Galactic extinction using Schlegel et al. (1998) maps) and corresponding error, integrated absolute  $V - I$  color (corrected for Galactic extinction) and corresponding error, and the projected separation from the center of its host galaxy  $d_{\text{proj}}$  in kiloparsecs. The numbers of GCCs located outside the isophote of constant surface brightness  $\mu_B \sim 26.5$  mag/arcsec<sup>2</sup> of the host galaxy are marked by an asterisk symbol (\*).

GCC	X, Y	RA (J2000) DEC	$r_h$	$e$	$V_0$	$(V - I)_0$	$d_{\text{proj}}$
DDO53-3-1120	291.022, 208.595	08 34 04.1 +66 10 23	6.7	0.2	-5.88 ± 0.07	1.39 ± 0.10	0.33
BK3N-2-863*	546.324, 579.284	09 54 00.1 +68 58 54	6.8	0.1	-5.23 ± 0.08	0.93 ± 0.11	1.34
KDG73-2-378*	377.384, 64.881	10 53 07.7 +69 32 02	8.3	0.1	-5.75 ± 0.08	1.11 ± 0.11	1.54
KK77-4-939	97.291, 330.684	09 50 00.3 +67 31 10	3.7	0.3	-5.01 ± 0.09	0.77 ± 0.12	1.25
KK77-4-1162	138.177, 568.545	09 49 56.2 +67 31 11	6.5	0.1	-5.37 ± 0.08	0.82 ± 0.11	1.61
KK77-4-1165	491.903, 572.199	09 49 54.8 +67 30 37	7.8	0.0	-5.69 ± 0.08	1.20 ± 0.11	1.60
KDG61-3-1325	363.770, 403.865	09 57 02.8 +68 35 35	4.7	0.1	-7.55 ± 0.07	0.92 ± 0.10	0.05
KDG63-3-1168	347.918, 329.025	10 05 07.2 +66 33 30	6.0	0.0	-7.09 ± 0.07	1.07 ± 0.10	0.17
DDO78-1-167	421.025, 524.751	10 26 28.3 +67 40 45	7.4	0.1	-7.23 ± 0.07	0.78 ± 0.10	1.46
DDO78-3-1082	483.889, 549.646	10 26 27.1 +67 39 10	7.0	0.1	-8.81 ± 0.07	0.96 ± 0.10	0.26
BK6N-2-524	225.256, 182.777	10 34 29.3 +66 01 29	4.4	0.3	-5.40 ± 0.08	1.18 ± 0.11	0.85
BK6N-4-789	608.148, 247.233	10 34 19.8 +66 00 32	4.5	0.3	-5.60 ± 0.07	1.45 ± 0.10	1.16
Garland-1-728	477.284, 107.876	10 03 30.8 +68 41 55	3.2	0.1	-8.26 ± 0.07	0.94 ± 0.10	1.23
HoIX-3-866	384.173, 122.948	09 57 37.7 +69 02 29	5.2	0.0	-7.89 ± 0.07	0.54 ± 0.10	0.52
HoIX-3-1168	596.137, 284.848	09 57 33.7 +69 02 14	4.0	0.3	-6.00 ± 0.08	0.30 ± 0.11	0.39
HoIX-3-1322	383.979, 347.673	09 57 33.7 +69 02 36	4.5	0.3	-6.00 ± 0.08	0.30 ± 0.11	0.14
HoIX-3-1565	376.681, 438.844	09 57 32.2 +69 02 39	4.1	0.1	-5.31 ± 0.08	0.74 ± 0.11	0.08
HoIX-3-1664	378.637, 471.226	09 57 31.6 +69 02 40	4.1	0.0	-6.20 ± 0.07	0.37 ± 0.10	0.12
HoIX-3-1932	264.772, 567.834	09 57 30.5 +69 02 54	9.4	0.3	-6.61 ± 0.07	0.71 ± 0.10	0.38
HoIX-3-2116	376.956, 643.274	09 57 28.5 +69 02 45	5.0	0.0	-7.26 ± 0.07	0.37 ± 0.10	0.40
HoIX-3-2129	155.863, 649.230	09 57 29.7 +69 03 06	5.1	0.1	-5.83 ± 0.08	0.38 ± 0.11	0.61
HoIX-3-2158	200.676, 656.790	09 57 29.3 +69 03 02	6.2	0.0	-6.98 ± 0.08	0.30 ± 0.11	0.57
HoIX-3-2373	558.027, 742.226	09 57 25.8 +69 02 31	7.9	0.1	-6.04 ± 0.08	1.31 ± 0.11	0.61
HoIX-3-2376	322.360, 744.024	09 57 27.1 +69 02 53	4.8	0.0	-5.90 ± 0.08	0.30 ± 0.11	0.59
HoIX-3-2409	266.049, 762.700	09 57 27.0 +69 02 59	3.8	0.2	-7.39 ± 0.07	0.68 ± 0.10	0.66
HoIX-4-1038	172.803, 269.307	09 57 40.0 +69 03 25	5.5	0.1	-9.05 ± 0.07	0.44 ± 0.10	1.23
HoIX-4-1085	307.374, 301.260	09 57 37.8 +69 03 32	3.8	0.1	-5.23 ± 0.09	0.48 ± 0.13	1.18
E540-030-4-1183*	150.605, 590.136	00 49 20.6 -18 02 51	6.2	0.1	-5.37 ± 0.08	1.24 ± 0.11	1.65
E294-010-3-1104	485.338, 317.674	00 26 32.6 -41 51 10	6.7	0.3	-5.32 ± 0.07	1.34 ± 0.10	0.14
KK027-4-721	435.879, 190.280	03 21 10.0 -66 18 26	7.5	0.0	-6.36 ± 0.07	1.15 ± 0.10	0.62
Sc22-2-879	108.743, 520.881	00 23 53.3 -24 41 39	12.2	0.2	-6.11 ± 0.08	1.15 ± 0.11	0.88
Sc22-2-100*	734.953, 661.836	00 23 55.5 -24 40 44	8.3	0.0	-5.90 ± 0.07	0.96 ± 0.11	2.17
Sc22-4-106*	598.857, 570.335	00 23 44.9 -24 42 09	4.9	0.2	-6.05 ± 0.07	0.96 ± 0.11	1.86
DDO113-2-579*	765.664, 227.122	12 14 52.8 +36 14 38	7.9	0.2	-5.60 ± 0.07	1.38 ± 0.10	1.54
DDO113-4-690	368.908, 76.646	12 14 54.4 +36 12 55	6.5	0.1	-5.27 ± 0.08	0.99 ± 0.11	0.61
U7605-3-1503	547.917, 423.740	12 28 39.9 +35 43 01	12.2	0.3	-6.44 ± 0.08	1.18 ± 0.11	0.38
KK109-3-1200*	538.659, 754.664	11 47 08.1 +43 40 28	4.4	0.2	-5.87 ± 0.08	0.92 ± 0.11	0.95
U7298-3-1280	741.363, 371.228	12 16 27.3 +52 13 09	4.6	0.1	-5.67 ± 0.08	0.66 ± 0.11	0.88
U8308-2-1198	145.016, 739.639	13 13 27.2 +46 19 23	7.5	0.0	-5.52 ± 0.08	1.08 ± 0.12	0.90
U8308-3-2040	39.610, 748.843	13 13 17.0 +46 19 07	9.1	0.1	-6.62 ± 0.08	1.46 ± 0.11	1.21
U8308-4-893*	663.358, 350.654	13 13 15.3 +46 19 32	5.1	0.1	-6.30 ± 0.07	1.55 ± 0.10	1.59
U8308-4-971*	699.289, 438.755	13 13 14.4 +46 19 35	8.3	0.1	-5.62 ± 0.09	1.20 ± 0.12	1.78
KK211-3-917	296.748, 173.889	13 42 08.0 -45 12 29	6.3	0.1	-6.86 ± 0.07	0.91 ± 0.10	0.48
KK211-3-149	429.726, 419.984	13 42 05.6 -45 12 20	6.1	0.2	-7.82 ± 0.07	0.95 ± 0.10	0
KK221-2-608	550.374, 168.636	13 48 54.9 -47 00 10	5.0	0.1	-8.04 ± 0.07	1.00 ± 0.10	1.78
KK221-2-883	404.756, 354.161	13 48 52.8 -47 00 19	8.3	0.1	-7.07 ± 0.07	1.00 ± 0.10	1.41
KK221-2-966	140.354, 399.808	13 48 50.3 -47 00 10	5.7	0.0	-9.80 ± 0.07	0.98 ± 0.10	0.90
KK221-2-1090	78.866, 479.706	13 48 49.4 -47 00 14	8.7	0.0	-7.77 ± 0.07	0.91 ± 0.10	0.77
KK221-3-1062	301.010, 266.780	13 48 48.2 -46 59 46	9.1	0.3	-6.10 ± 0.08	0.93 ± 0.11	0.37
KK200-3-1696	785.776, 763.252	13 24 32.2 -30 58 11	9.2	0.1	-5.68 ± 0.09	1.03 ± 0.12	1.17
KK84-2-785	173.139, 447.814	10 05 35.8 -07 44 08	11.6	0.0	-7.30 ± 0.08	1.00 ± 0.11	2.46
KK84-2-974	432.320, 678.779	10 05 37.5 -07 43 44	14.9	0.0	-6.64 ± 0.09	0.57 ± 0.14	3.82
KK84-3-705	460.100, 105.800	10 05 35.7 -07 44 26	9.2	0.1	-7.45 ± 0.08	1.04 ± 0.11	1.66
KK84-3-830	395.303, 454.705	10 05 35.1 -07 44 60	10.6	0.1	-9.68 ± 0.07	0.96 ± 0.10	0
KK84-3-917	624.322, 609.065	10 05 36.5 -07 45 17	10.4	0.1	-7.52 ± 0.08	1.06 ± 0.11	1.29
KK84-4-666	538.305, 207.182	10 05 31.5 -07 45 04	10.6	0.0	-8.37 ± 0.07	1.26 ± 0.10	2.45
KK84-4-789	290.956, 379.188	10 05 30.5 -07 44 38	19.4	0.3	-7.08 ± 0.08	0.88 ± 0.12	3.48
KK84-4-967	571.750, 560.942	10 05 29.1 -07 45 04	12.0	0.2	-6.81 ± 0.08	0.95 ± 0.12	4.10
U9240-3-4557	545.377, 491.651	14 24 45.0 +44 31 36	3.6	0.2	-7.22 ± 0.07	0.61 ± 0.10	0.19
KK112-3-976	447.781, 261.936	11 54 43.3 -33 33 44	9.1	0.1	-5.93 ± 0.08	1.25 ± 0.11	0.28
KK112-4-742	183.817, 164.666	11 54 47.3 -33 33 23	11.8	0.1	-6.21 ± 0.08	0.88 ± 0.11	1.48
KK112-4-792	444.689, 215.677	11 54 46.6 -33 32 58	15.0	0.1	-6.77 ± 0.08	1.22 ± 0.11	1.43
E490-017-3-1769	306.876, 462.734	06 37 57.0 -26 00 08	6.6	0.2	-7.06 ± 0.08	0.30 ± 0.11	0.05
E490-017-3-1861	246.213, 480.112	06 37 57.3 -26 00 13	6.4	0.1	-7.38 ± 0.07	0.87 ± 0.10	0.16
E490-017-3-1956	507.111, 498.721	06 37 57.0 -25 59 48	5.1	0.3	-5.37 ± 0.09	0.55 ± 0.13	0.37
E490-017-3-2035	374.045, 514.220	06 37 57.3 -26 00 00	7.1	0.3	-7.30 ± 0.07	0.41 ± 0.11	0.12
E490-017-3-2509	657.358, 639.546	06 37 57.7 -25 59 30	8.4	0.2	-5.69 ± 0.08	1.10 ± 0.11	0.75



Table 2. –continued.

GCC	X, Y	RA (J2000) DEC	$r_h$	$e$	$V_0$	$(V - I)_0$	$d_{\text{proj}}$
KK065–3–1095	290.890, 434.702	07 42 29.4 +16 34 29	11.5	0.1	$-6.75 \pm 0.08$	$1.41 \pm 0.11$	0.33
U4115–2–1042	190.123, 708.172	07 57 04.9 +14 22 25	11.9	0.3	$-6.00 \pm 0.08$	$1.03 \pm 0.12$	1.72
U4115–3–784	614.000, 125.730	07 57 03.8 +14 22 43	9.4	0.1	$-7.53 \pm 0.07$	$0.93 \pm 0.11$	1.19
U4115–4–1477	607.416, 740.185	07 57 04.1 +14 24 58	8.0	0.0	$-5.37 \pm 0.10$	$0.91 \pm 0.16$	2.63
UA438–3–2004	299.313, 413.097	23 26 28.3 –32 23 06	3.7	0.2	$-8.67 \pm 0.07$	$0.96 \pm 0.10$	0.16
UA438–3–3325	733.228, 621.063	23 26 26.7 –32 23 49	3.7	0.1	$-5.96 \pm 0.07$	$1.02 \pm 0.10$	0.41
U3755–2–652	378.719, 209.939	07 13 50.1 +10 32 15	5.5	0.1	$-8.22 \pm 0.07$	$0.98 \pm 0.10$	1.84
U3755–2–675	107.413, 234.823	07 13 50.4 +10 31 48	8.1	0.1	$-5.75 \pm 0.09$	$1.19 \pm 0.12$	1.21
U3755–2–863	61.125, 358.956	07 13 51.2 +10 31 44	5.2	0.1	$-6.93 \pm 0.08$	$1.03 \pm 0.11$	0.96
U3755–3–727	494.971, 57.246	07 13 52.1 +10 31 43	9.5	0.1	$-7.21 \pm 0.10$	$0.60 \pm 0.15$	0.85
U3755–3–739	467.346, 64.840	07 13 51.9 +10 31 42	5.7	0.2	$-8.67 \pm 0.07$	$0.85 \pm 0.10$	0.83
U3755–3–754	380.674, 72.749	07 13 51.3 +10 31 41	8.1	0.0	$-6.47 \pm 0.09$	$0.56 \pm 0.14$	0.82
U3755–3–768	404.724, 81.923	07 13 51.5 +10 31 40	5.7	0.2	$-5.42 \pm 0.10$	$1.05 \pm 0.17$	0.79
U3755–3–914	379.331, 139.121	07 13 51.3 +10 31 34	9.5	0.0	$-7.60 \pm 0.08$	$0.64 \pm 0.11$	0.65
U3755–3–974	434.698, 161.008	07 13 51.7 +10 31 32	7.0	0.1	$-5.70 \pm 0.01$	$0.53 \pm 0.16$	0.58
U3755–3–1045	390.476, 186.888	07 13 51.4 +10 31 29	8.3	0.3	$-6.01 \pm 0.10$	$0.45 \pm 0.16$	0.53
U3755–3–1182	393.821, 228.672	07 13 51.5 +10 31 25	7.9	0.2	$-8.54 \pm 0.07$	$0.56 \pm 0.10$	0.43
U3755–3–1256	483.184, 249.602	07 13 52.1 +10 31 24	8.6	0.0	$-7.77 \pm 0.07$	$0.97 \pm 0.10$	0.37
U3755–3–1257	511.799, 250.293	07 13 52.3 +10 31 24	6.2	0.0	$-8.71 \pm 0.07$	$0.97 \pm 0.10$	0.40
U3755–3–1364	354.699, 277.022	07 13 51.2 +10 31 20	6.0	0.1	$-7.00 \pm 0.08$	$0.49 \pm 0.12$	0.36
U3755–3–1611	318.852, 334.848	07 13 51.0 +10 31 14	7.5	0.0	$-7.48 \pm 0.08$	$0.83 \pm 0.11$	0.34
U3755–3–1616	615.652, 335.551	07 13 53.0 +10 31 16	7.5	0.2	$-6.40 \pm 0.09$	$0.69 \pm 0.12$	0.46
U3755–3–1732	195.199, 365.183	07 13 50.2 +10 31 11	10.0	0.1	$-6.09 \pm 0.08$	$1.01 \pm 0.11$	0.62
U3755–3–1737	466.051, 366.036	07 13 52.0 +10 31 12	8.3	0.2	$-6.71 \pm 0.08$	$1.05 \pm 0.11$	0.09
U3755–3–1963	453.046, 423.153	07 13 51.9 +10 31 06	9.1	0.1	$-6.46 \pm 0.09$	$0.56 \pm 0.14$	0.09
U3755–3–2027	369.997, 444.823	07 13 51.4 +10 31 04	6.3	0.2	$-5.80 \pm 0.10$	$0.60 \pm 0.15$	0.22
U3755–3–2123	530.273, 487.378	07 13 52.5 +10 31 00	6.5	0.1	$-7.76 \pm 0.07$	$0.42 \pm 0.11$	0.33
U3755–3–2168	363.214, 511.255	07 13 51.4 +10 30 57	8.7	0.2	$-7.63 \pm 0.07$	$1.00 \pm 0.10$	0.36
U3755–3–2204	496.118, 528.265	07 13 52.3 +10 30 56	6.6	0.1	$-6.07 \pm 0.09$	$0.82 \pm 0.13$	0.37
U3755–3–2334	637.259, 611.302	07 13 53.3 +10 30 49	6.7	0.1	$-6.90 \pm 0.07$	$0.51 \pm 0.11$	0.74
U3755–3–2363	471.076, 639.739	07 13 52.2 +10 30 45	8.3	0.0	$-7.75 \pm 0.07$	$0.49 \pm 0.10$	0.63
U3755–3–2368	526.825, 646.637	07 13 52.5 +10 30 45	7.0	0.3	$-7.44 \pm 0.07$	$0.53 \pm 0.11$	0.68
U3755–3–2398	555.514, 670.612	07 13 52.7 +10 30 43	8.5	0.3	$-6.17 \pm 0.09$	$1.13 \pm 0.13$	0.76
U3755–3–2401	392.910, 676.091	07 13 51.6 +10 30 41	12.0	0.0	$-7.54 \pm 0.07$	$0.97 \pm 0.10$	0.73
U3755–3–2403	231.105, 677.272	07 13 50.5 +10 30 40	6.8	0.0	$-6.79 \pm 0.07$	$0.92 \pm 0.10$	0.89
U3755–3–2408	496.303, 682.668	07 13 52.3 +10 30 41	8.6	0.0	$-6.89 \pm 0.08$	$0.43 \pm 0.11$	0.75
U3755–3–2459	457.060, 743.123	07 13 52.1 +10 30 35	8.3	0.0	$-7.98 \pm 0.07$	$0.57 \pm 0.10$	0.89
U3755–4–566	188.706, 59.303	07 13 48.9 +10 31 27	8.6	0.3	$-6.25 \pm 0.09$	$0.87 \pm 0.14$	1.31

- James, P. A., Shane, N. S., Knapen, J. H., Etherton, J., & Percival, S. M. 2005, *A&A*, 429, 851
- Jerjen, H., Binggeli, B., & Barazza, F. D. 2004, *AJ*, 127, 771
- Jordán, A., Côté, P., West, M. J., & Marzke, R. O. 2002, *ApJL*, 576, L113
- Karachentsev, I. D., Karachentseva, V. E., Huchtmeier, W. K., & Makarov, D. I. 2004, *AJ*, 127, 2031
- Karachentsev, I. D., et al. 2003, *A&A*, 398, 467
- Karachentsev, I. D., et al. 2001a, *A&A*, 363, 117
- Karachentsev, I. D., et al. 2001b, *A&A*, 379, 407
- Karachentsev, I. D., et al. 2001c, *A&A*, 375, 359
- Karachentsev, I. D., et al. 2000, *ApJ*, 542, 128
- King, I. 1962, *AJ*, 67, 471
- Kissler-Patig, M. 2000, *Reviews of Modern Astronomy*, 13, 13
- Klypin, A., Kravtsov, A. V., Valenzuela, O., & Prada, F. 1999, *ApJ*, 522, 82
- Kravtsov, A. V., Gnedin, O. Y., & Klypin, A. A. 2004, *ApJ*, 609, 482
- Kundu, A., & Whitmore, B. C. 2001a, *AJ*, 121, 2950
- Kundu, A., & Whitmore, B. C. 2001b, *AJ*, 122, 1251
- Lada, C. J., & Lada, E. A. 2003, *ARA&A*, 41, 57
- Larsen, S. S. & Richtler, T. 2000, *A&A*, 354, 836
- Larsen, S. S., Brodie, J. P., Huchra, J. P., Forbes, D. A., & Grillmair, C. J. 2001, *AJ*, 121, 2974
- Lotz, J. M., Telford, R., Ferguson, H. C., Miller, B. W., Stiavelli, M., & Mack, J. 2001, *ApJ*, 552, 572
- Lotz, J. M., Miller, B. W., & Ferguson, H. C. 2004, *ApJ*, 613, 262
- Makarova, L. N. 1999, *A&A*, 139, 491
- Makarova, L. N., et al. 1998, *A&A*, 128, 459
- Marlowe, A. T., Meurer, G. R., & Heckman, T. M. 1999, *ApJ*, 522, 183
- Mateo, M. 1998, *ARA&A*, 36, 435
- Miller, B., Lotz, J., Hilker, M., Kissler-Patig, M., Puzia, T., & Stiavelli, M. 2004, *AAS Meeting Abstracts*, 204
- Minniti, D., Meylan, G., & Kissler-Patig, M. 1996, *A&A*, 312, 49
- Pelupessy, F. I., van der Werf, P. P., & Icke, V. 2004, *A&A*, 422, 55
- Puzia, T. H., Kissler-Patig, M., Brodie, J. P., & Huchra, J. P. 1999, *AJ*, 118, 2734
- Puzia, T. H., et al. 2004, *A&A*, 415, 123
- Puzia, T. H., Perrett, K. M., & Bridges, T. J. 2005, *A&A*, 434, 909
- Searle, L., & Zinn, R. 1978, *ApJ*, 225, 357
- Secker, J. 1992, *AJ*, 104, 1472
- Schlegel, D.J., Finkbeiner, D.P., Davis M., 1998, *ApJ* 500, 525
- Silverman, B. W. 1986, *Density Estimation for Statistics and Data Analysis*, Chap and Hall/CRC Press, Inc.
- Stetson, P. B. 1987, *PASP*, 99, 191
- Strader, J., Brodie, J.P., Forbes, D.A., Beasley, M.A., and Huchra, J.P. 2003, *AJ*, 125, 1291
- Surdin, V.G., Arkhipova, N.A., 1998, *Russian Astronomy Letters*, 24, 343
- van den Bergh, S. 2000, *ApJ*, 530, 777
- van den Bergh, S., & Mackey, A. D. 2004, *MNRAS*, 354, 713
- de Vaucouleurs, G., de Vaucouleurs, A., Corwin, H. G. Jr., Buta, R., Paturel, G., and Fouque, P. 1991, *Third Reference*

- Catalogue of bright galaxies, Berlin: Springer
- Weilbacher, P. M. 2002, Ph.D. Thesis
- Whitmore, B. C., Zhang, Q., Leitherer, C., Fall, S. M.,  
Schweizer, F., & Miller, B. W. 1999, AJ, 118, 1551
- Yun, M. S., Ho, P. T. P., & Lo, K. Y. 1994, Nature, 372, 530

**Table 3.** The King law approximation parameters for globular cluster candidates in nearby LSB dwarf galaxies. The table contains the following columns: identifier of each cluster (as in Table 2), reddening corrected  $V$ -band central surface brightness in mag/arcsec<sup>2</sup> and corresponding error, reddening corrected  $I$ -band central surface brightness in mag/arcsec<sup>2</sup> and corresponding error, King core radius  $r_c$  and corresponding error, King tidal radius  $r_t$  and corresponding error, and the King concentration parameter  $c=r_t/r_c$ .

GCC	$\mu_{V,0}$	$\mu_{I,0}$	$r_c$	$r_t$	$c$
DDO53-3-1120	20.92 ± 0.08	19.67 ± 0.01	4.16 ± 0.09	21.3 ± 1.0	5.2
BK3N-2-863*	20.95 ± 0.13	20.70 ± 0.03	2.38 ± 0.38	26.4 ± 4.5	11.1
KDG73-2-378*	21.33 ± 0.05	20.09 ± 0.03	3.47 ± 0.21	124.:	36.0
KK77-4-939	20.64 ± 0.68	20.44 ± 0.07	2.26 ± 0.22	17.1 ± 3.4	7.6
KK77-4-1162	21.03 ± 0.04	20.35 ± 0.05	2.78 ± 0.18	18.0 ± 2.4	6.5
KK77-4-1165	21.42 ± 0.05	20.46 ± 0.17	3.19 ± 0.22	15.9 ± 0.7	5.0
KDG61-3-1325	18.45 ± 0.03	17.59 ± 0.05	1.88 ± 0.06	33.8 ± 2.7	18.0
KDG63-3-1168	18.93 ± 0.04	18.14 ± 0.03	1.90 ± 0.06	53.4 ± 11.2	28.1
DDO78-1-167	18.69 ± 0.11	17.75 ± 0.03	3.53 ± 0.14	46.7 ± 6.8	13.2
DDO78-3-1082	17.93 ± 0.04	16.98 ± 0.02	2.89 ± 0.06	34.6 ± 2.1	12.0
BK6N-2-524	20.40 ± 0.13	20.04 ± 0.05	1.54 ± 0.15	90.2 ± 56.7	58.7
BK6N-4-789	20.47 ± 0.11	19.66 ± 0.01	1.91 ± 0.18	68.0 ± 8.1	34.9
Garland-1-728	16.76 ± 0.04	15.90 ± 0.08	0.69 ± 0.00	42.3 ± 14.6	61.0
HoIX-3-866	17.88 ± 0.07	18.14 ± 0.11	1.51 ± 0.06	42.3 ± 7.1	28.0
HoIX-3-1168	19.69 ± 0.07	19.71 ± 0.42	2.00 ± 0.15	12.3 ± 1.1	6.2
HoIX-3-1322	20.02 ± 0.01	20.37 ± 0.08	2.34 ± 0.00	18.0 ± 0.5	7.7
HoIX-3-1565	19.34 ± 0.31	19.10 ± 0.64	1.06 ± 0.44	16.8 ± 7.4	13.5
HoIX-3-1664	19.28 ± 0.11	19.17 ± 0.39	1.18 ± 0.09	116. ± 87.2	98.0
HoIX-3-1932	20.06 ± 0.03	19.60 ± 0.07	3.50 ± 0.15	23.0 ± 2.6	6.6
HoIX-3-2116	18.53 ± 0.19	18.65 ± 0.06	2.18 ± 0.14	21.4 ± 3.0	8.7
HoIX-3-2129	20.42 ± 0.17	20.30 ± 0.21	2.09 ± 0.45	975.:	466.1
HoIX-3-2158	19.41 ± 0.04	19.44 ± 0.07	3.69 ± 0.28	11.8 ± 0.9	3.2
HoIX-3-2373	21.11 ± 0.03	19.70 ± 0.06	3.17 ± 0.31	22.3 ± 2.6	7.1
HoIX-3-2376	19.60 ± 0.30	20.34 ± 0.16	1.46 ± 0.46	76.3:	52.4
HoIX-3-2409	18.31 ± 0.12	17.91 ± 0.03	1.91 ± 0.06	14.4 ± 0.5	7.5
HoIX-4-1038	17.06 ± 0.10	16.81 ± 0.11	2.08 ± 0.19	27.1 ± 3.9	13.1
HoIX-4-1085	20.24 ± 0.27	20.50 ± 0.40	1.40 ± 0.29	18.3 ± 4.8	13.2
E540-030-4-1183*	21.13 ± 0.02	20.15 ± 0.03	2.92 ± 0.09	28.3 ± 2.9	9.7
E294-010-3-1104	20.96 ± 0.05	19.52 ± 0.06	3.64 ± 0.50	17.0 ± 3.3	4.7
KK027-4-721	20.39 ± 0.09	19.55 ± 0.03	3.33 ± 0.11	41.1 ± 4.9	12.3
Scu22-2-879	22.08 ± 0.04	20.77 ± 0.05	6.06 ± 0.62	51.3 ± 16.9	8.5
Scu22-2-100*	20.72 ± 0.04	20.29 ± 0.03	3.44 ± 0.20	22.2 ± 2.2	6.5
Scu22-4-106*	20.12 ± 0.10	19.44 ± 0.07	1.91 ± 0.18	33.4 ± 7.0	17.5
DDO113-2-579*	21.26 ± 0.05	19.53 ± 0.03	2.73 ± 0.14	14.1 ± 1.3	5.2
DDO113-4-690	21.32 ± 0.02	20.18 ± 0.07	3.74 ± 0.19	19.4 ± 2.4	5.2
U7605-3-1503	21.49 ± 0.07	20.48 ± 0.05	6.16 ± 0.71	80.3 ± 79.7	13.1
KK109-3-1200*	19.94 ± 0.17	19.40 ± 0.20	1.70 ± 0.22	19.2 ± 3.0	11.3
U7298-3-1280	20.56 ± 0.16	19.88 ± 0.45	2.42 ± 0.45	16.1 ± 4.6	6.7
U8308-2-1198	21.61 ± 0.03	20.17 ± 0.06	2.78 ± 0.20	27.4 ± 3.7	9.9
U8308-3-2040	20.62 ± 0.08	19.07 ± 0.03	3.25 ± 0.17	34.2 ± 15.2	10.5
U8308-4-893*	20.03 ± 0.02	18.54 ± 0.06	1.91 ± 0.00	66.9 ± 5.8	35.0
U8308-4-971*	21.83 ± 0.06	20.64 ± 0.02	3.68 ± 0.30	132. ± 50.0	36.2
KK211-3-917	19.55 ± 0.04	18.98 ± 0.03	2.54 ± 0.12	51.9 ± 13.9	20.5
KK211-3-149	18.99 ± 0.03	18.18 ± 0.05	2.98 ± 0.12	113. ± 51.9	38.1
KK221-2-608	18.03 ± 0.03	17.50 ± 0.08	1.78 ± 0.06	49.4 ± 3.9	27.8
KK221-2-883	20.04 ± 0.03	19.30 ± 0.04	3.43 ± 0.17	71.4 ± 28.8	20.8
KK221-2-966	16.57 ± 0.04	15.90 ± 0.06	2.26 ± 0.11	46.0 ± 6.2	20.4
KK221-2-1090	19.17 ± 0.04	18.58 ± 0.02	3.57 ± 0.09	30.6 ± 3.3	8.6
KK221-3-1062	21.77 ± 0.06	21.00 ± 0.06	5.85 ± 0.85	43.1 ± 21.5	7.4
KK200-3-1696	21.48 ± 0.06	20.87 ± 0.04	4.25 ± 0.42	38.0 ± 13.2	9.0
KK84-2-785	20.25 ± 0.12	19.69 ± 0.13	4.54 ± 0.50	39.9 ± 5.3	8.8
KK84-2-974	21.48 ± 0.10	21.08 ± 0.04	5.31 ± 0.61	38.5 ± 3.9	7.3
KK84-3-705	21.41 ± 0.33	20.03 ± 0.10	10.6 ± 1.86	36.8 ± 14.1	3.4
KK84-3-830	18.19 ± 0.03	17.16 ± 0.10	3.19 ± 0.18	90.4 ± 4.0	28.4
KK84-3-917	20.56 ± 0.10	19.62 ± 0.17	4.84 ± 0.43	40.9 ± 4.7	8.5
KK84-4-666	19.32 ± 0.07	18.44 ± 0.03	3.81 ± 0.18	45.3 ± 1.8	11.9
KK84-4-789	21.59 ± 0.14	20.94 ± 0.10	6.85 ± 1.56	57.7 ± 34.1	8.4
KK84-4-967	21.50 ± 0.05	20.61 ± 0.14	9.90 ± 1.12	22.2 ± 1.7	2.3
U9240-3-4557	18.37 ± 0.01	17.64 ± 0.10	1.81 ± 0.00	20.2 ± 0.8	11.2
KK112-3-976	21.03 ± 0.03	20.28 ± 0.05	3.37 ± 0.12	40.6 ± 5.3	12.1
KK112-4-742	21.40 ± 0.06	20.76 ± 0.05	4.64 ± 0.41	68.8 ± 38.5	14.8
KK112-4-792	21.26 ± 0.03	19.99 ± 0.02	6.20 ± 0.20	41.9 ± 3.6	6.8
E490-017-3-1769	19.49 ± 0.03	19.33 ± 0.10	3.16 ± 0.15	38.6 ± 6.9	12.2
E490-017-3-1861	18.86 ± 0.08	18.24 ± 0.04	2.76 ± 0.12	28.8 ± 3.8	10.5
E490-017-3-1956	20.85 ± 0.28	20.59 ± 0.01	2.74 ± 0.09	22.8 ± 26.9	8.3
E490-017-3-2035	19.23 ± 0.03	18.80 ± 0.06	3.27 ± 0.18	38.5 ± 15.2	11.8
E490-017-3-2509	21.00 ± 0.01	20.38 ± 0.04	4.79 ± 0.09	16.5 ± 0.4	3.5

**Table 3.** – continued.

GCC	$\mu_{V0}$	$\mu_{I0}$	$r_c$	$r_t$	$c$
KK065-3-1095	20.96 ± 0.03	19.50 ± 0.01	5.28 ± 0.12	55.3 ± 6.0	10.5
U4115-2-1042	21.74 ± 0.08	21.07 ± 0.07	4.89 ± 0.71	293.:	59.9
U4115-3-784	19.82 ± 0.14	19.21 ± 0.09	3.11 ± 0.48	64.6 ± 38.7	20.8
U4115-4-1477	21.74 ± 0.36	20.96 ± 0.05	4.23 ± 0.38	25.7 ± 5.1	6.1
UA438-3-2004	17.05 ± 0.01	16.10 ± 0.04	1.73 ± 0.04	33.3 ± 2.6	19.3
UA438-3-3325	19.42 ± 0.08	18.62 ± 0.03	1.67 ± 0.06	31.2 ± 19.8	18.7
U3755-2-652	17.78 ± 0.06	17.19 ± 0.03	1.78 ± 0.27	33.5 ± 7.7	18.9
U3755-2-675	21.20 ± 0.05	20.24 ± 0.34	4.36 ± 0.38	18.6 ± 1.9	4.3
U3755-2-863	19.11 ± 0.15	18.92 ± 0.02	1.77 ± 0.20	42.6 ± 2.8	24.1
U3755-3-727	20.19 ± 0.08	19.82 ± 0.03	4.04 ± 0.20	141. ± 97.5	35.1
U3755-3-739	18.00 ± 0.09	17.37 ± 0.03	2.30 ± 0.09	67.8 ± 7.6	29.5
U3755-3-754	20.34 ± 0.05	20.20 ± 0.09	3.93 ± 0.51	25.0 ± 6.1	6.4
U3755-3-768	20.98 ± 0.21	21.08 ± 0.25	2.25 ± 0.41	38.0 ± 15.7	17.0
U3755-3-914	19.84 ± 0.04	20.06 ± 0.03	3.43 ± 0.18	94.1 ± 46.2	27.5
U3755-3-974	21.22 ± 0.04	20.82 ± 0.03	3.47 ± 0.20	15.7 ± 5.5	4.5
U3755-3-1045	21.30 ± 0.08	21.02 ± 0.09	5.63 ± 1.41	17.5 ± 4.8	3.1
U3755-3-1182	18.39 ± 0.02	18.06 ± 0.02	3.54 ± 0.09	33.1 ± 1.9	9.4
U3755-3-1256	19.49 ± 0.05	18.82 ± 0.01	4.13 ± 0.09	36.6 ± 1.5	8.9
U3755-3-1257	17.74 ± 0.03	17.24 ± 0.03	2.15 ± 0.09	35.4 ± 1.8	16.5
U3755-3-1364	19.49 ± 0.22	19.52 ± 0.08	2.73 ± 0.27	283.:	103.9
U3755-3-1611	19.29 ± 0.05	18.82 ± 0.06	2.70 ± 0.12	38.3 ± 4.9	14.2
U3755-3-1616	20.83 ± 0.12	20.39 ± 0.07	3.12 ± 0.48	60.7 ± 32.7	19.5
U3755-3-1732	21.04 ± 0.08	20.37 ± 0.08	3.89 ± 0.50	60.9 ± 48.9	15.7
U3755-3-1737	20.17 ± 0.04	19.95 ± 0.05	3.02 ± 0.15	34.6 ± 4.5	11.5
U3755-3-1963	20.91 ± 0.12	20.70 ± 0.10	4.50 ± 1.03	90.4:	20.1
U3755-3-2027	20.85 ± 0.04	20.98 ± 0.05	3.53 ± 0.20	16.6 ± 1.0	4.7
U3755-3-2123	19.22 ± 0.05	19.18 ± 0.11	2.62 ± 0.12	344.:	131.4
U3755-3-2168	19.54 ± 0.03	18.93 ± 0.03	4.18 ± 0.18	27.1 ± 2.0	6.5
U3755-3-2204	20.81 ± 0.15	20.27 ± 0.04	2.98 ± 0.12	19.8 ± 6.4	6.7
U3755-3-2334	19.90 ± 0.05	19.57 ± 0.05	3.34 ± 0.22	20.1 ± 2.0	6.0
U3755-3-2363	19.05 ± 0.08	18.86 ± 0.07	3.00 ± 0.27	39.7 ± 9.4	13.3
U3755-3-2368	19.82 ± 0.02	19.59 ± 0.01	3.35 ± 0.09	33.4 ± 2.0	10.0
U3755-3-2398	21.39 ± 0.03	20.77 ± 0.06	7.04 ± 0.48	18.0 ± 1.1	2.6
U3755-3-2401	19.92 ± 0.04	19.63 ± 0.02	4.07 ± 0.22	42.0 ± 3.0	10.3
U3755-3-2403	20.00 ± 0.06	19.11 ± 0.10	3.20 ± 0.22	20.0 ± 2.0	6.3
U3755-3-2408	20.21 ± 0.06	20.12 ± 0.05	3.59 ± 0.31	66.8 ± 36.7	18.6
U3755-3-2459	18.65 ± 0.04	18.74 ± 0.05	2.62 ± 0.09	49.0 ± 5.1	18.7
U3755-4-566	21.23 ± 0.03	20.59 ± 0.06	4.87 ± 0.33	53.6 ± 19.4	11.0